TEMPERATURE EFFECTS ON THE ANGULAR CORRELATION OF POSITRON ANNIHILATION RADIATION IN SOLIDS

By

LEWIS PORTER KELLER

Bachelor of Science

Valparaiso University

Valparaiso, Indiana

1960

Submitted to the faculty of the Graduate School of
the Oklahoma State University
in partial fulfillment of the requirements
for the degree of
MASTER OF SCIENCE
August, 1962

OKLAHOMA
STATE UNIVERSITY
LIBRARY

NOV 8 1962

TEMPERATURE EFFECTS ON THE ANGULAR CORRELATION
OF POSITRON ANNIHILATION RADIATION IN SOLIDS

Thesis Approved:

B. Clark Grosecloss
Thesis Adviser

J. E. Harrington

Dean of the Graduate School

504530

PREFACE

In the most probable type of electron-positron annihilation, two .51 Mev gamma rays are emitted in nearly opposite directions. The slight angular deviation of the two photons from 180° is caused by the motion of the center of mass of the electron-positron pair. An angular correlation experiment measures the angular distribution of the annihilation photons, and from this measured distribution one can obtain information about the motion of the electrons in the solid. Changing the temperature of the solid changes the angular distribution of the annihilation radiation. This is due to a change in the amount of positronium formed in the solid. With the exception of crystalline quartz, the solids studied were amorphous materials.

The author wishes to thank the following persons for aid in conducting this research:

Dr. B. C. Groseclose for continous aid and encouragement during the execution of this work.

Mr. G. D. Loper for helpful discussions.

Mr. Heinz Hall, Mr. Richard Gruhlkey, and Mr. Frank Hargrove for work on the apparatus.

Beatrice Keller for typing the manuscript.

This work was supported in part by an Army contract.

TABLE OF CONTENTS

LIST OF TABLES

LIST OF FIGURES

CHAPTER I

INTRODUCTION

A. General Remarks

An angular correlation experiment is one in which studies are made of events such as electron-positron annihilation or fission by measuring the angles at which the decay products are emitted. Such an experiment can be performed for events in which two or more decay products are emitted simultaneously. In this type of experiment it is then possible to correlate the data with the state of the system just before decay or annihilation.

The study of electron-positron annihilation by the method of angular correlation was first suggested by DuMond, et. al. (1) in 1949. At that time it was pointed out that it might be possible to determine electron velocities in metals using this method. Since then a number of investigators have observed the angular distribution of the annihilation photons in a variety of substances besides metals. (Review articles have been written by Berko and Hereford (2) and by Wallace (3).)

According to the present theory, an annihilation of an electron-positron pair can occur either from a free state or from a bound state, which is called positronium. When a positron enters a material, it begins slowing down due to collisions with the atoms of the material. As it is slowing down, it may either capture an electron to form positronium

or it may reach thermal energy (.025 ev) in a free state. A very small percentage of positrons are annihilated before they reach thermal energies (4). It has been shown that positrons either form positronium (5,6) or reach thermal energies in a time which is short compared to the mean lifetime (7). The lifetimes of the bound state and free state are essentially the same.

The lifetime is very dependent on the relative spin of the annihilating pair in both the free state annihilation and the bound state annihilation. If the spins of the two particles are in opposite directions, giving a total spin of zero (singlet state), a two photon annihilation occurs and the mean lifetime is about 1.25×10^{-10} seconds and is nearly independent of the material in which the annihilation takes place (8). If the spins of the two particles are in the same direction, giving a total spin of one (triplet state), a three photon annihilation occurs and the mean lifetime is about 1.4×10^{-7} seconds and is also nearly independent of the material in which the positrons annihilate (9). This means that the cross section for the singlet state annihilation is more than two orders of magnitude larger than the cross section for triplet state annihilation. (When one speaks of a singlet state annihilation, it must be remembered that unless otherwise specified, this can mean annihilation from a free singlet state or from a bound singlet state. Also, triplet state annihilation can mean annihilation from a free triplet state or a bound triplet state. Another point that should be kept in mind is that when one speaks of the lifetime of a certain state, this means the average or mean lifetime.)

Nothing has yet been said about how it is possible to know whether an annihilation has taken place from a free state or from a bound state.

There are, however, differences between the two types of annihilation. For instance, in a free singlet state annihilation, the electron usually has appreciable kinetic energy while the positron is most probably thermalized. To conserve energy and momentum the two phtons will not be emitted in exactly opposite directions but will have a slight angular deviation from 180 degrees. However, in a bound singlet state annihilation it is most probable that the positronium will be slowed down to energies of the order of 0.5 ev (5), so that to conserve energy and momentum the two photons will be emitted very nearly 180 degrees apart. An angular correlation experiment would be able to measure these angular differences and thereby show which type of annihilation took place. Actually, since an experiment cannot pinpoint one particular annihilation but can only give data for a large number of annihilations, then it is possible to tell only the percent of positrons which annihilate in a free state and the percent which annihilate from a bound state.

B. Positronium

Before discussing the types of annihilation of an electron-positron pair it is essential that the basic properties of the bound state of these particles be understood. This state is similar to a hydrogen atom except that the reduced mass, $\mu = \frac{m_1 m_2}{m_1 + m_2}$, is one-half of the reduced mass of a hydrogen atom. This has the effect of changing the possible bound energy states to one-half their value for hydrogen and doubling the radii of the Bohr orbits. The expressions for the possible bound energy states and the Bohr radii are respectively,

$$W_n = -\frac{1}{4}\frac{m_o e^4}{\hbar^2 n^2}$$

and

$$a_n = \frac{2n^2\hbar^2}{m_o e^2},$$

where

m_o = rest mass of electron = 9.1×10^{-28} gm.

e = charge of electron = 4.80×10^{-10} esu.

$\hbar = \frac{h}{2\pi} = 1.052 \times 10^{-27}$ erg sec.

n = principal quantum number = 1, 2, 3, ...

For the ground state in which n = 1,

$$W_1 = -6.8 \text{ ev}$$

$$a_1 = 10.6 \times 10^{-8} \text{ cm.}$$

Also, for each value of n and ℓ, an additional splitting arises due to the interaction of the magnetic moments of the electron and positron. This is normally called hyperfine structure and in this case has a much larger effect since the magnetic moment of the positron is larger than the magnetic moments of nuclei. The magnitude of the hyperfine splitting for S states is given by (10)

$$W_m = \left(\frac{8\pi}{3}\right) \mu^2 \, \bar{\sigma}_1 \cdot \bar{\sigma}_2 \, |\psi(0)|^2,$$

where

μ = magnetic moment of electron and positron

$\bar{\sigma}_1$ = Pauli spin operator for positron

$\bar{\sigma}_2$ = Pauli spin operator for electron

$\bar{\sigma}_1 \cdot \bar{\sigma}_2 = -3$ (singlet state)

$\bar{\sigma}_1 \cdot \bar{\sigma}_2 = 1$ (triplet state)

$\psi(0)$ = wave function for hydrogen atom for S states with m_o replaced by $\frac{m_o}{2}$ and evaluated at r = 0 to give $\frac{1}{\sqrt{\pi}} \left(\frac{me^2}{2n\hbar^2}\right)^{3/2}$.

Substituting these values into the expression for W_m gives

$$W_m = \frac{\alpha^4}{12} \cdot \frac{mc^2}{n^3} \text{ (triplet states)}$$

and

$$W_m = -\frac{\alpha^4}{4} \cdot \frac{mc^2}{n^3} \text{ (singlet states),}$$

where

$$\alpha = \frac{e^2}{\hbar c} .$$

This shows that for a given n and for $\ell = 0$, the triplet state lies above the singlet state. For $n = 1$,

$$\Delta W_m = \frac{4}{12} \alpha^4 mc^2 .$$

A splitting of the same order of magnitude is caused by the annihilation force which arises from the fact that the $^3S_1$ positronium spends part of the time in a virtual one-photon state (10). This gives a splitting between triplet and singlet of

$$\Delta W_a = \frac{3}{12} \alpha^4 mc^2 .$$

Therefore

$$\Delta W = \Delta W_m + \Delta W_a = \frac{7}{12} \alpha^4 mc^2 = 8.45 \times 10^{-4} \text{ ev.}$$

This value for the singlet-triplet splitting is for the $n = 1$, $\ell = 0$ state. It will decrease by a factor $\frac{1}{n^3}$ for higher values of n.

In order to calculate the lifetime of the singlet state the cross section for two photon decay is needed. This has been derived by Dirac (11) and is

$$\sigma_{2\gamma} = \pi \left(\frac{e^2}{mc^2}\right)^2 \left(\frac{c}{v}\right) .$$

This expression holds for low velocities, for which the cross section obeys the $\frac{1}{v}$ law. The probability per second of a two photon annihilation is proportional to $\sigma_{2\gamma}$ and the probability that the positron lies in a unit volume in the immediate neighborhood of the electron (12). The probability per second of an annihilation will be independent of the velocity since the initial kinetic energy is very much less than the energy available for the process (12). Therefore,

$$P_{2\gamma} = 4 \sigma_{2\gamma} v \left|\psi(0)\right|^2 ,$$

where $\psi(0)$ is the wave function for the ground state of the positronium evaluated at r = 0. The factor four appears because Dirac's calculation of the cross section considered that a singlet collision (free state) or singlet positronium occurred only one-fourth of the time, whereas Wheeler is considering that a singlet collision has already occurred or that singlet positronium has already been formed. Therefore, the probability per second of two photon annihilation, which is defined as the reciprocal of the mean lifetime, becomes

$$P_{2\gamma} \equiv \frac{1}{\tau_{2\gamma}} = 4\pi \left(\frac{e^2}{mc^2}\right)^2 \left(\frac{c}{v}\right) \cdot v \cdot \frac{1}{\pi} \left(\frac{me^2}{2n\hbar^2}\right)^3$$

or

$$\tau_{2\gamma} = \frac{2\hbar n^3}{mc^2\alpha^5} = 1.25 \times 10^{-10} \text{ sec.}$$

Also, Ore and Powell (13) have shown that the probability per second of a three photon annihilation from the triplet state is given by

$$P_{3\gamma} \equiv \frac{1}{\tau_{3\gamma}} = \sigma_{3\gamma} v \left|\psi(0)\right|^2 = \frac{4}{9\pi}(\pi^2 - 9)\alpha \cdot \underbrace{\sigma_{2\gamma} v \left|\psi(0)\right|^2}_{1/\tau_{2\gamma}}$$

or

$$\tau_{3\gamma} = \frac{\tau_{2\gamma}}{\frac{4}{9\pi}(\pi^2 - 9)\alpha} = 1.4 \times 10^{-7} \text{ sec.}$$

The cross section for three photon annihilation from the triplet state can also be calculated from the above expression and is

$$\sigma_{3\gamma} = \frac{4}{9\pi}(\pi^2 - 9)\alpha\, \sigma_{2\gamma}.$$

The ratio of the two cross sections $\sigma_{2\gamma}$ and $\sigma_{3\gamma}$ is

$$\frac{\sigma_{2\gamma}}{\sigma_{3\gamma}} = \frac{\sigma_{2\gamma}}{\frac{4}{9\pi}(\pi^2 - 9)\alpha\, \sigma_{2\gamma}} = 1115,$$

but since this does not take into account that the triplet state is formed three times as often as the singlet state, then the actual ratio of two photon annihilations to three photon annihilations is

$$\frac{2\gamma}{3\gamma} = \frac{1}{3}\frac{\sigma_{2\gamma}}{\sigma_{3\gamma}} = 372.$$

These calculations of the two different lifetimes and the ratio of two photon annihilation to three photon annihilation agree well with experiment for materials in which little or no positronium is formed (8, 9, 14). However, for materials in which positronium is formed the ratio $\frac{2\gamma}{3\gamma}$ decreases considerably (15), and about 30% of the positrons annihilate with a lifetime between $\tau_{2\gamma}$ and $\tau_{3\gamma}$ (8). This intermediate mean lifetime, called the τ_2 component, has a value on the order of 2×10^{-9} seconds. It was first suggested by Dresden (16) that τ_2 arose from an annihilation of the positron in triplet positronium with an electron of opposite spin which is bound to a molecule. This type of annihilation is commonly called "pickoff" annihilation and occurs only in materials in which positronium is formed.

In order for positronium to be formed in a substance, there must be sufficient room in the lattice structure or between the molecules for the positronium atom to exist. It is now recognized that little or no positronium will be formed in a substance unless it has an "Ore gap" (5). This is the energy region between the lowest excitation potential of an electron in the molecule, and the lowest ionization energy of the molecule minus the binding energy of positronium (Figure 1). When a positron enters the material with a large kinetic energy (average kinetic energy equals 360 kev for positrons from a Na^{22} source (17)), it causes ionizations in the material and loses energy rapidly by elastic and inelastic collisions. There is very little positronium formed in this high energy range because the positron has too large a velocity to hold an electron. When the positron slows down enough so that its kinetic energy is less than the lowest ionization energy of the

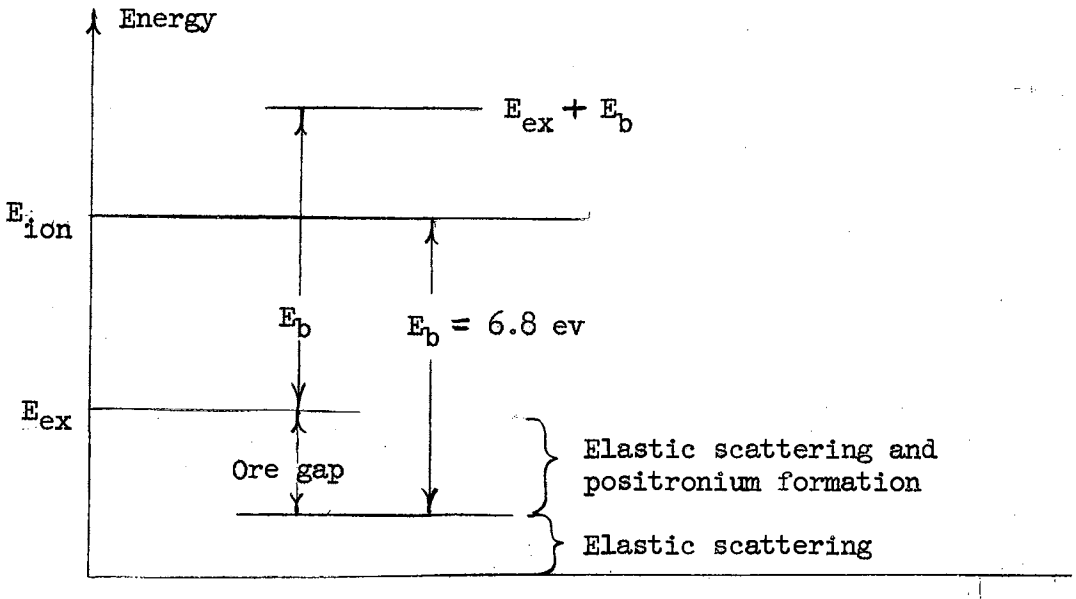

Figure 1. Energetics of Positronium Formation

surrounding atoms, it can only excite electrons in the atoms to the various higher energy levels. In this range of energy between the ionization energy and lowest excitation energy, the positron has enough binding energy (6.8 ev ground state) to overcome the ionization energy of some of the electrons and form positronium, but the most probable process is electron excitation (5). When the positron's kinetic energy decreases below the lowest excitation potential, it is probable that positronium will be formed if the binding energy is large enough to remove an electron. When the kinetic energy gets below the ionization energy minus the binding energy, positronium cannot be formed since the positron's binding energy would not be sufficient to remove the electron. If the positron has still not captured an electron, it will experience elastic collisions until it is thermalized and then annihilate in the free state. There is also the possibility that it will be excited back into the Ore gap.

It must be remembered that in molecular substances in which positronium is formed there are a large number of ionization and excitation energies so that the situation is not as simple as has been described here. Also, vibrational modes of molecules hinder positronium formation (3). Even though the overall picture in a molecular substance is very complicated, the above description and diagram holds for any particular electron bound to a molecule. In metals where there are free electrons it would seem that a large percent of the positrons would form positronium. The reason this does not happen is that the lattice spacing in metals is too small to allow room for the positronium to exist (3).

The probability of positronium being formed in higher S states, is small since the radius of the positronium atom increases by n^2. If, however, higher S states are formed, the previous calculation shows that the lifetime with respect to annihilation increases as the cube of the principal quantum number. Even though radiative transitions between singlet and triplet S states are forbidden (18), transitions from excited S states to the singlet ground state are possible with lifetimes on the order of 10^{-7} to 10^{-9} seconds (13). Therefore, if free positronium is formed in an excited S state, the observed lifetime may be essentially the time required for spontaneous de-excitation to the singlet ground state. Ore and Powell (13) have pointed out that the transition from $2S \rightarrow 1S$ is absolutely forbidden due to the symetry selection rule. However, Wallace (19) shows that the 2S state would not possess the spherical symetry needed to make it a metastable state and therefore transitions could be expected in times on the order of the measured positron lifetime. Excitation from the ground state to higher S states is improbable since the first excited state is 5 ev above the ground

state. If the positronium is formed in higher ℓ states (P,D, etc.), the probability of annihilation is small since $\psi(r)$ approaches zero as $r \rightarrow 0$ for $\ell \neq 0$. From this discussion it can be concluded that most of the annihilations are from the $n=1, \ell=0$ singlet state or the $n=1, \ell=0$ triplet state.

C. Types of Annihilation

Previously it has been stated without proof that singlet S states annihilate via two photon emission and triplet S states annihilate via three photon emission. The proof of these two statements is given by De Benedetti and Corben (10), Wallace (3), and Jauch and Rohrlich (20). The following is a summary of their arguments. The state $^3S_1$, $J = 1$, must be represented by three functions (corresponding to the three m states) which transform as components of a vector or of a pseudovector. (Components of a vector have odd parity and components of a pseudovector have even parity.) Now consider two quanta traveling in opposite directions. This state must be symetrical under the exchange of the two photons, but since neither vector or pseudovector states can satisfy this requirement, the $^3S_1$ state cannot annihilate by 2γ emission, and therefore 3γ annihilation is most probable. (Single quantum annihilation will be discussed later, but it is a very improbable process.) On the other hand the $^1S_0$ state can be represented by either a scaler or a pseudoscaler depending on whether the parity of the two particles is even or odd. Since both the scaler and pseudoscaler are symetrical under the exchange of the two photons, the $^1S_0$ state can annihilate by 2γ emission. Since it has been observed experimentally that the annihilation quanta are plane polarized in planes perpendicular to each other, showing a pseudoscaler final state, the $^1S_0$ state is

pseudoscaler; so that the parity of the electron is opposite that of the positron.

To prove that the ^1S_o state cannot annihilate with an odd number of photons, DeBenedetti and Corben consider the operation of charge conjugation, i.e. change in sign of all electric charges and all electromagnetic fields. For the positron-electron pair the charge conjugation operator is equivalent to charge exchange alone since there are no electromagnetic fields present. Also the charge exchange operation is equivalent to parity times spin exchange. This is shown in the following diagrams.

Initial State Parity Exchange Parity x Spin Exchange

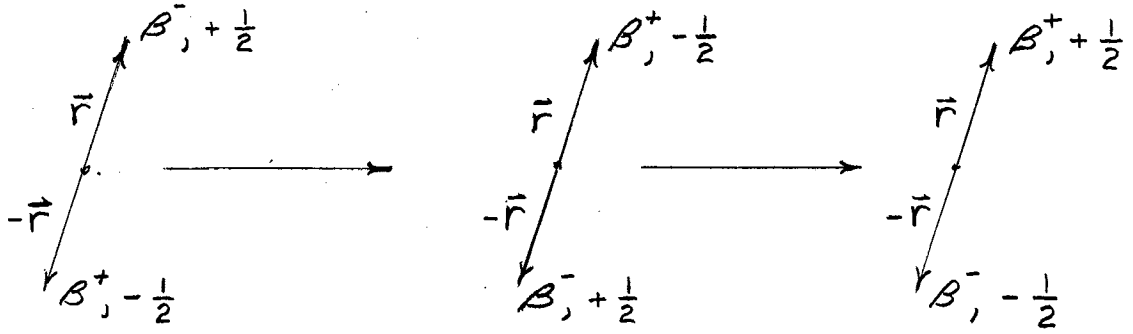

This final state, parity times spin exchange, is seen to differ from the initial state in that the charges on each particle have been exchanged. Now, since the singlet state is odd with respect to spin exchange and has odd parity (pseudoscaler), it is even with respect to charge conjugation. In the final state each gamma ray photon has a polarization state $\vec{\mathcal{E}}$ and the charge conjugation operator reverses the sign of each vector $\vec{\mathcal{E}}$ (electromagnetic radiation), so that the eigenvalue of the charge conjugation operator is $(-1)^n$ for a final state of n quanta. Therefore since the ^1S_o state is even with respect to charge conjugation it can annihilate with only an even number of quanta.

Similarily the $^3S_1$ state can annihilate with only an odd number of quanta.

Single quantum annihilation is excluded by the laws of conservation of momentum unless the annihilation takes place while a third particle is closely interacting with the annihilating pair and will take up the surplus recoil momentum (12). Usually the third particle would be the nucleus of an atom in the substance and since Coulomb repulsion keeps positrons away from the nuclei, single quantum annihilation with the nucleus as the third particle is not a common process. The interacting particle can also be another electron or another positron. Wallace (3) has shown that this process is also unlikely.

D. Angular Correlation and Some Previous Experimental Results

As was stated previously, in a two photon annihilation the photons travel in nearly opposite direction and have energies which are nearly equal to m_oc^2 where m_o is the rest mass of the electron. The reason the angle between the photons is not exactly 180 degrees or the energy of each photon is not exactly m_oc^2 is that the center of mass of the annihilating pair usually is not stationary. Even thermal motions will give slight deviations from 180 degrees and m_oc^2. A typical angular correlation experimental arrangement is shown in Figure 2. This type of apparatus measures only the Z component of the center of mass momentum. This component, p_z, is given by

$$p_z = mc(\pi - \alpha) = mc\theta,$$

where

α = angle between the two photons

θ = angle of deviation from 180 degrees.

A typical value is $\Theta = 10$ milliradians giving $p_z = 27 \times 10^{-20}$ gm.cm./sec. which corresponds to $E = \frac{p_z^2}{4m_o} = 13$ ev. The factor four appears in the denominator of the expression for E since the mass of the positron-electron pair is $2m_o$.

The deviation of the energy of the gamma rays from $m_o c^2$, caused by the motion of the center of mass in the x direction producing a Doppler effect, is difficult to measure accurately. Its magnitude for a 5 ev electron moving in the x direction at the time of annihilation is 1.1 kev compared to $m_o c^2 = 510$ kev (21).

In 1949 DeBenedetti, Cowan, Konneker, and Primakoff (22) measured the distribution of gamma pairs arising from annihilations in Au. The observed angular distribution indicated that the mean energy of the annihilating pairs was about 15 ev. They assumed that the positron was thermalized, so that the conduction electrons must have this mean energy. (No core electrons participate since nuclei repel positrons.) Green and Stewart (23) made angular correlation measurements on various metals and the data show that for most metals the distribution curves are inverted parabolae with tails at large angles. Some metals (for example Au and Cu)

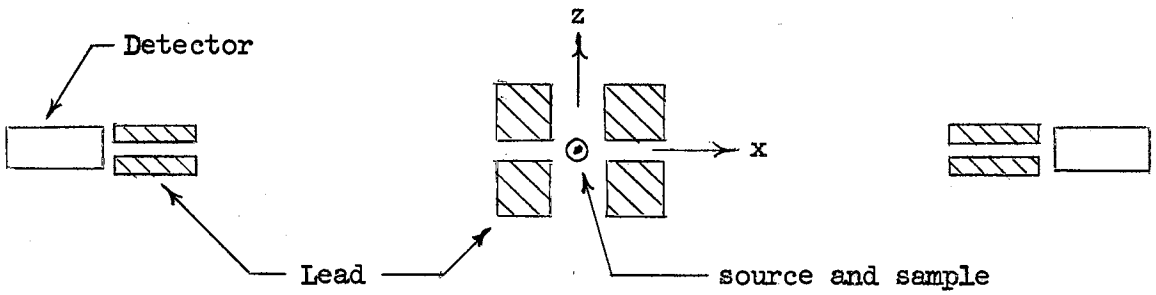

Figure 2. Geometry of an Angular Correlation Experiment

have a bell-shaped angular distribution. Page, Heinburg, Wallace, and Trout (24) have obtained angular correlation data for a molecular material (fused quartz) which exhibits a very narrow component. They calculated that fused quartz has a half-width of 3 milliradians for the narrow component and $\sim$11 milliradians for the broad component. The narrow component is attributed to singlet positronium which has been thermalized. R. deZafra and W. Joyner (6) have measured the effects of temperature, pressure, irradiation, and phase change on the angular distribution of the annihilation radiation from some molecular substances that exhibit the τ_2 component of lifetime, and hence a narrow component. They reported that the percentage of annihilations contributing to the narrow component increases with increasing temperature, decreases with increasing pressure, and does not change after irradiation with a high neutron flux. As to phase change, substances whose density decreases with a change in phase (for example napthalene) have more annihilations in the narrow component after the change. For substances whose density increases with a change in phase (for example ice $\rightarrow$ water), more narrow component annihilations are present before the change. They conclude that these changes in the percentage of annihilations in the narrow component are due to changes in density: if the density increases, less positronium is formed, and the percentage decreases; if the density decreases, more positronium is formed, and the percentage increases.

It should be made clear that the process which gives rise to the τ_2 component of lifetime (i.e. pickoff annihilation) is not the process which gives rise to a narrow component in angular correlation experiments. The electron which is involved in pickoff annihilation usually has a large enough energy so that the annihilation falls in the broad component. The τ_2 lifetime and the narrow component are related

only in that they both depend on positronium formation.

Page and Heinberg (25) have performed a magnetic quenching experiment (placed the sample in a high magnetic field) on several substances which exhibit a narrow component. The results show that for Teflon and polyethylene, 3 to 4% of the annihilation events are transferred to the narrow component. This is interperted as a conversion of ^3S positronium to ^1S positronium in a time short compared to the τ_2 lifetime. A magnetic field (16 kilogauss) was also applied to Cu and Mg, which do not show a narrow component, and there was no change in the shape of the curve taken for zero magnetic field. This was expected since it is assumed that little or no positronium is formed in these materials.

Brandt, Berko, and Walker (26) have interpreted the increase of annihilations in the narrow component with increase in temperature as due to a free volume effect; i.e. as the temperature increases the free volume increases, so that pickoff annihilation occurs more from the (outer) low momentum electrons.

CHAPTER II

APPARATUS

A. Physical Arrangement

The physical setup consisted of three main parts. These were the stationary slit, the source holder and the movable slit. These parts are best described by Figures 3, 4, and 5. Figure 3 shows the stationary slit formed by two lead bricks with the photomultiplier tube and pre-amplifier mounted behind the slit. A 2" x 2" cylindrical sodium iodide scintillator is mounted on the end of the photomultiplier tube. The steel base plate has three leveling screws and its dimensions are 25" x 15" x 3/8". The leveling screws are set into three steel disks which are 1/2" thick and 3" in diameter. In order for the stationary slit and scintillator to be at the same height as the source and the moving slit, the three disks are set on iron bricks which rest on the table. Since the weight of this entire assembly is large, the iron bricks were not fastened to the table.

The two machined lead bricks which define the slit have dimensions of 6" x 4" x 1". They are mounted such that the slit width can be adjusted between 0 and 6 millimeters and so that the position of the slit can be adjusted in the Z direction (see Figure 2).

In the center section (Figure 4) the steel base plate is exactly the same as the one described previously, except that the steel disks are set directly on the table. Since the base plate supports a large

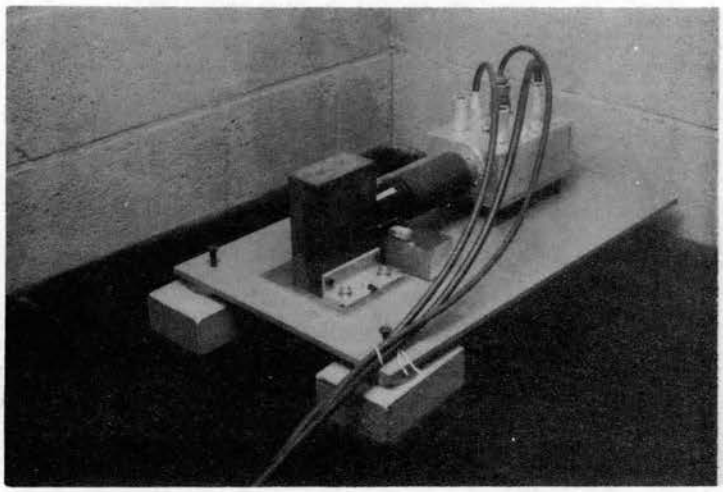

Figure 3. Stationary Slit.

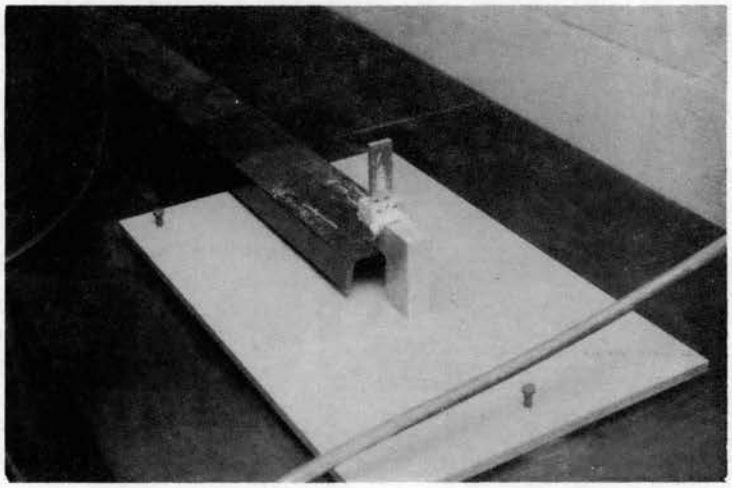

Figure 4. Source and Mounting.

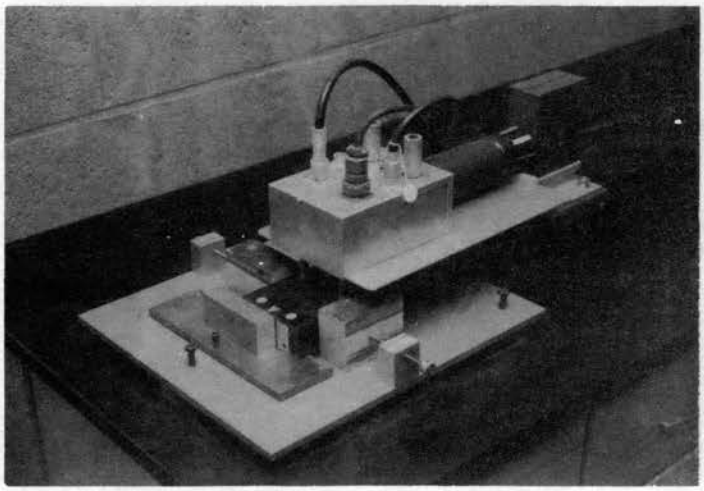

Figure 5. Movable Slit.

amount of lead shielding, which has a considerable weight, it was not necessary to fasten the supporting disks to the table. The L-shaped aluminum piece which is mounted in the center of the base plate supports the source holder and also serves as the support for the long aluminum beam. The beam is held in place by a flat head screw which goes up through the beam and into the aluminum center piece as shown in Figure 4 . This screw also serves as the pivot point for the beam.

The source and sample holder (shown in Figure 4) was designed so as to take advantage of all positrons emitted by the Na^{22} (see Figure 6 for the Na^{22} γ-ray spectrum). About 10 milligrams of $Na^{22}Cl$ which had an activity between .5 and 1 millicurie was evaporated in a needle shaped strip of dimensions 3.8cm x .25cm on a piece of .2 mil mylar. This was covered by a similiar piece of mylar and positioned in the source holder with the long dimension in the vertical direction. The samples to be tested were then placed in the holder on each side of the source, so that all positrons are emitted into the sample. Actually about 20% of the annihilations occur in the source itself and in the mylar, so that a background curve must be taken with no sample in the holder, and this curve must be subtracted from the curves obtained with samples. However, this method still gives a larger count rate than if the source was set to one side; so that only the positrons emitted in one hemisphere could annihilate in the sample material. The holder was constructed so that it could be tilted or "plumbed" to make sure that the source would be vertical. The holder could also be adjusted back and forth in the Z direction to make sure it would be on a line between the two slits (at position zero).

The base plate which supports the moving end of the aluminum beam also has three leveling screws and supporting disks. A smaller and

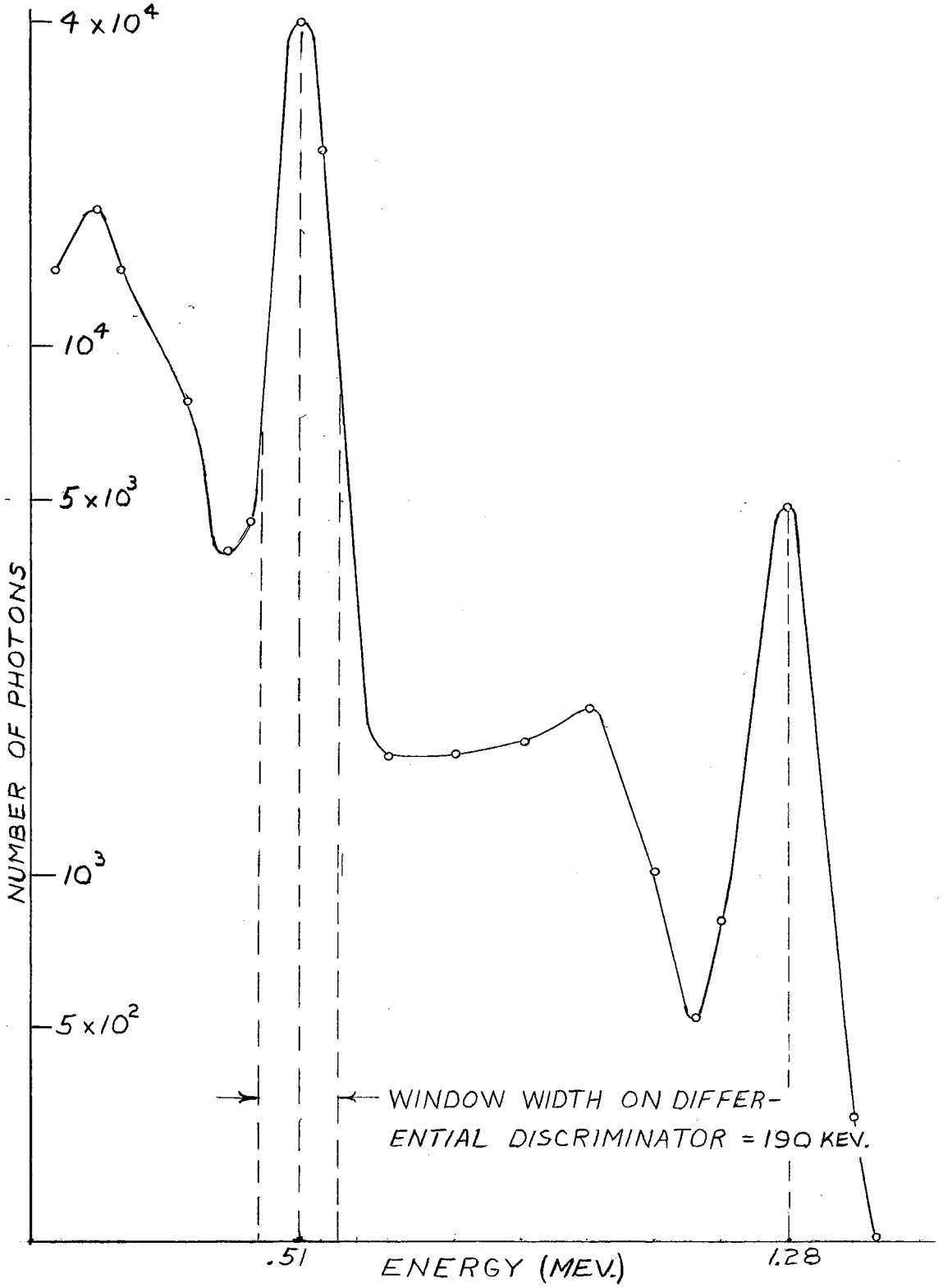

Figure 6. Na^{22} Gamma Ray Spectrum

smoother steel plate with a separate set of leveling screws is set at the far end of the base plate and serves as the "runway" for the rotating beam. The beam rolls on small roller bearings which are set into its end as shown in Figure 5. The small plate also supports the scale which is marked in milliradians. The beam is rotated and held in place by two long screws mounted horizontally, one on each side. By tightening one screw and loosening the other, the position of the beam can be set with precision. The scintillator, photomultiplier tube, and pre-amplifier are mounted on the movable beam as shown. The lead bricks which define the slit are mounted in front of the scintillator and can be adjusted in a manner similiar to the adjustment of the slit at the stationary end.

B. Temperature Apparatus

The samples were heated and cooled by means of a brass apparatus which could be slipped onto the source holder from above (see Figure 7).

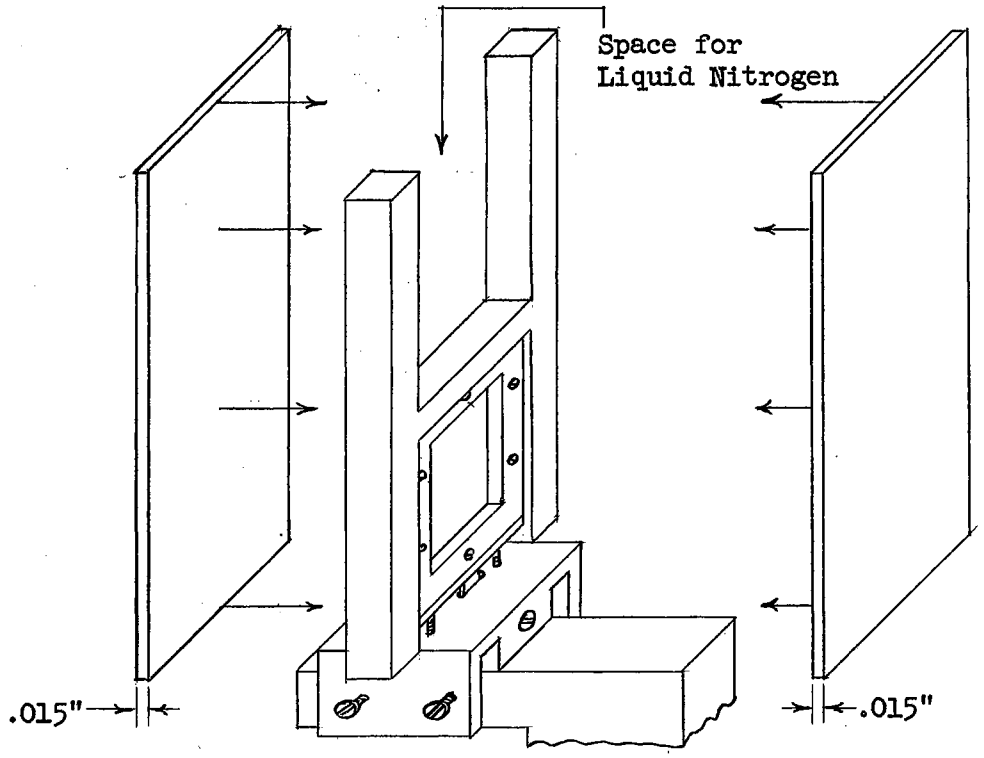

Figure 7. Temperature Apparatus

The brass made contact with the sides and top of the source holder, but did not touch the samples. This temperature apparatus was constructed by soldering two .015" brass plates onto an H shaped brass piece. The plates were made very thin since they were in the path of the annihilation photons. Approximately 5% of the annihilation radiation was absorbed in these thin plates. A heating wire was cemented to the upper part of the apparatus with Saureisen electric resistor cement and the whole piece was wrapped with asbestus insulation. For heating, a piece of brass was placed into the upper cavity and for cooling, a long rectangular tube was fitted into the upper cavity so that about 130 cubic inches of liquid nitrogen could be poured into the tube and upper cavity combined. The advantage of using this method as compared to placing the sample in a dewar flask filled with liquid nitrogen is that the alignment of the sample does not need to be changed. Also the count rate is higher than if the annihilation photons had to penetrate the liquid nitrogen and the walls of the dewar. The main disadvantage is that this device must be refilled frequently with liquid nitrogen. A thermocouple wire was imbedded into the sample to measure the temperature of the sample after it had come to equilibrium with the temperature apparatus. The source holder was insulated from its support by a piece of asbestus.

C. Electronics

A block diagram of the electronics used is shown in Figure 8. The photomultipliers used were the RCA 6342A type. The high voltage power supplies were Hamner N-401's and were operated at 1250 volts. The amplifiers were Victoreen Model 851A. A differential pulse height selector is built into each amplifier, so that one may discriminate

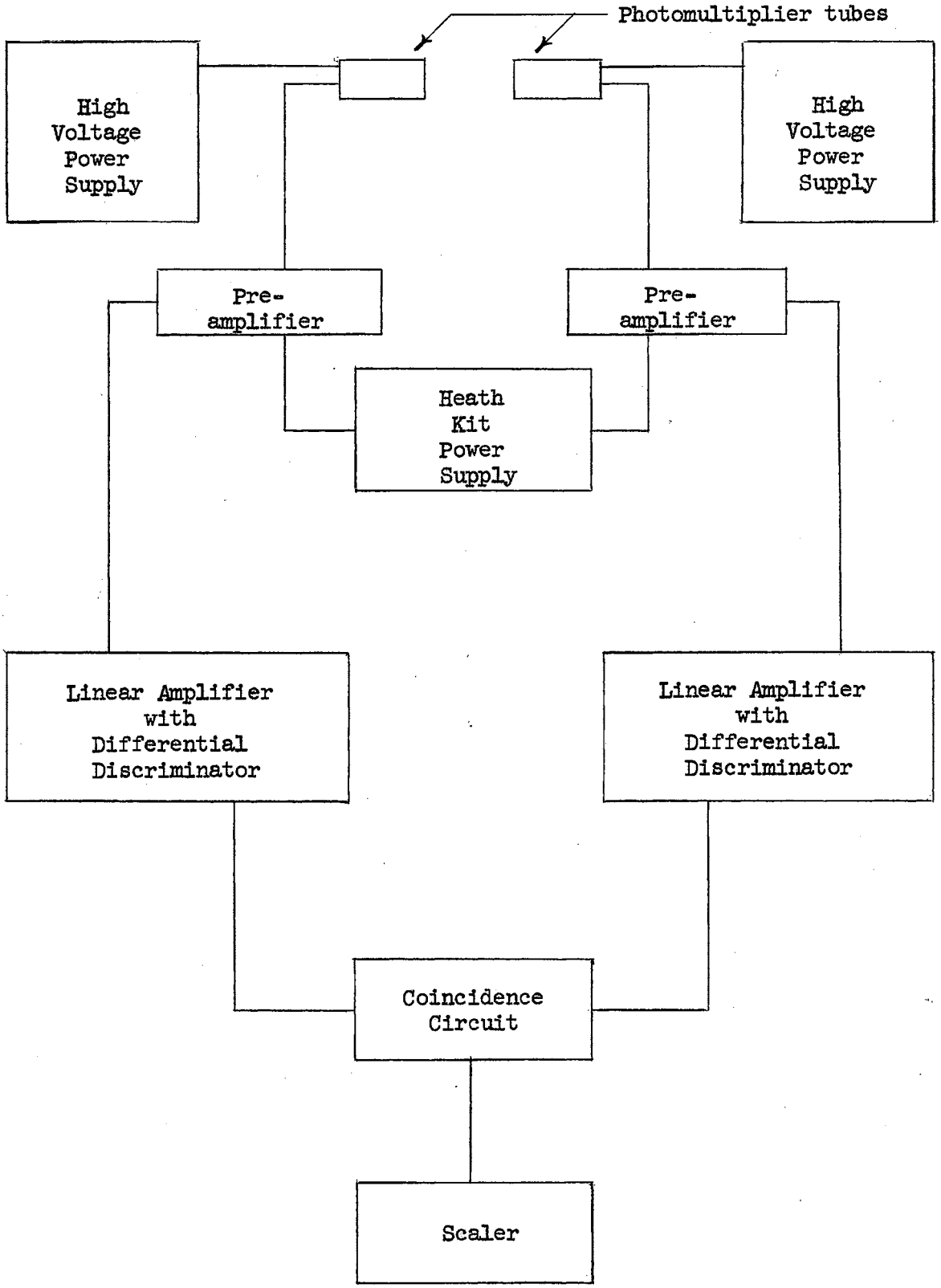

Figure 8. Block Diagram of the Circuit

against all photons except the ones with energies in a certain energy region. The output pulse of the pulse height selector was positive 24 volts. A replica of the Advance Radiation Engineering Corporation Model 401 Coincidence-Anticoincidence Analyzer was used. This circuit has a resolving time of 2 microseconds as determined by performing an experiment with two separate sources and counting the chance coincidences. The resolving time was then determined using the relation (27)

$$N_{ch} = 2\tau R_1 R_2,$$

where

N_{ch} = number of chance coincidence counts

τ = resolving time of circuit

R_1 and R_2 = singles counting rates.

The output pulse of the coincidence circuit was 25 volts positive. This was fed into a TMC model SG-3A2 scaler which also had a discriminator. This discriminator was set so that it would accept a 25 volt pulse. The line voltage for each instrument described was regulated by a Sola Constant Voltage Transformer.

CHAPTER III

COLLECTION OF DATA AND EXPERIMENTAL RESULTS

A. Collection of Data

Figures 10-13 show the angular distribution curves for Lucite, crystalline quartz, fused quartz, Teflon, and polystyrene. These curves have been normalized to the same area as the curve for Teflon taken at room temperature. The Teflon curve was chosen as the standard since it was obtained by using the same resolving time of the coincidence circuit that was used for the background curve. The background curve was corrected for horizontal and vertical resolution of the apparatus (see Appendix B), although in this case these corrections were hardly noticeable. The procedure for obtaining the curves which are shown was as follows:

(1) The chance coincidence background was subtracted from each point of the original data. This background was assumed to be the same at each position and was obtained by counting the number of coincidences at the 40 milli-radian position.

(2) The curve was then corrected for horizontal and vertical resolution and normalized to include the same area as the corrected room temperature Teflon curve. The areas under each curve were computed using Simpson's rule for

numerical integration. Each point of each curve was then multiplied by the appropriate constant so as to reduce all areas to the area under the Teflon curve. Multiplying each point of a particular curve by the same constant does not change the shape of the curve.

(3) This normalized curve was then plotted on tracing paper and the paper folded so that the two sides of the curve coincided. This was done because slight inaccuracies in alignment of the apparatus caused the peak of the curve to be shifted slightly off zero. This method was an accurate way of pinpointing the position of the peak of the curve. The curve was then shifted so that its peak coincided with the zero position, and the corrected background curve was subtracted.

(4) The area under each curve was then recalculated to make sure that all areas were equal.

The error bars shown were computed using the relation

$$\sigma = \sqrt{\sigma_a^2 + \sigma_b^2} \,,$$

where σ_a and σ_b are the standard deviations of the count rate with and without the sample. The standard deviation of a count rate is given by

$$\sigma_a = \frac{\sqrt{N}}{t}$$

where N = number of counts

t = counting time.

All curves shown have at least 3000 counts per point in the peak and a

proportionately smaller number in the wings. Due to the low counting rates (about 12 counts per minute at position zero) the time needed for each sample was about eight days. (The low temperature Lucite and polystyrene curves required less time as will be explained in Section B.) Therefore, to minimize the effects of drifts in the electronics, the position of the movable counter was changed frequently and with no set pattern. The data for angles greater than 10 milliradians were usually obtained overnight; and it was found that even though the percent error was larger than at the peak, the absolute error was hardly noticeable.

A background curve was also taken at 165°C, and after normalizing it to the area under the room temperature background curve; the two curves were very nearly identical (see Figure 9). About the only factor which could have caused a detectible change was a change in the amount of positronium formed in the source and aluminum coated mylar. At room temperature and at 165°C the lattice spacing of these materials would be too small for a positronium atom to exist. The background curve was not taken at liquid nitrogen temperature, but it will be assumed, using the above reasoning, that its shape does not change noticeably at low temperature. The slight change which might be caused by the mylar surrounding the source would not be noticed since the background is only about 20% of the measured distribution.

B. The Temperature Effect

Figures 10(a), 11(a), and 12(a) show the effects of temperature changes in Teflon, polystyrene, and Lucite. Figures 10(b), 11(b), and 12(b) are difference curves obtained by subtracting the low temperature data from the high temperature data. In Figure 10(b) the central area above the dotted line represents the change in the narrow component,

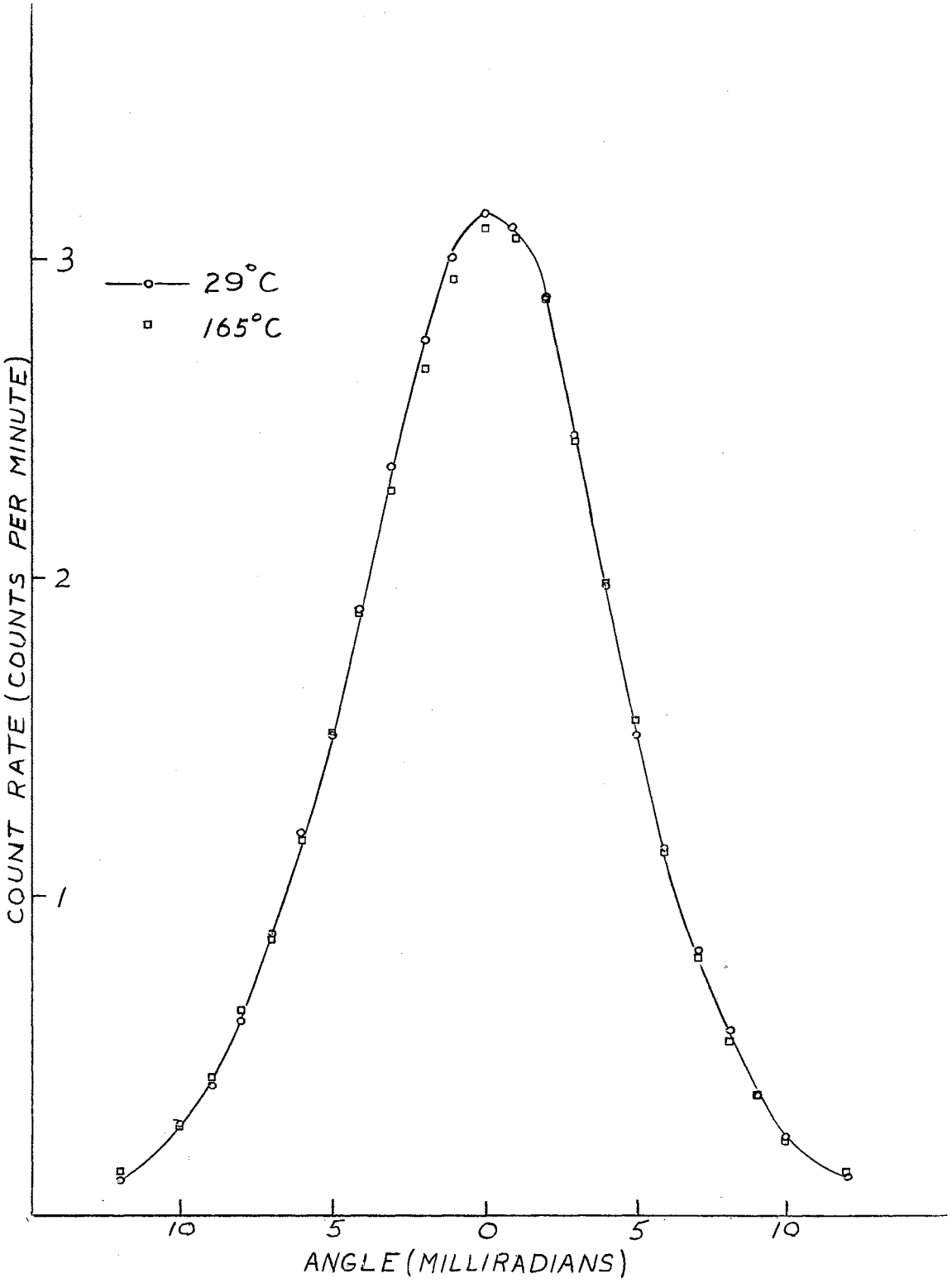

Figure 9. Angular Distribution of Background Radiation at 29°C and 165°C

while the total area under the zero line represents the change in the broad component. This is more easily seen by noticing that the coincidences which were originally detected in regions I and II (large angles) have been shifted to region III (small angles). Since the individual high and low temperature curves were normalized to equal areas, the combined area of regions I and II must equal the area of region III. Also contributing to the change in the narrow component are the annihilation photons which originally had a large deviation from 180 degrees (broad component) but were detected in the small angle positions; and now, due to the temperature change, have a small angular deviation from 180 degrees (narrow component) and are again detected in the small angle positions. (This is possible due to the large vertical dimensions of the slits. See Appendix B, part A.) Therefore the dotted line across the bottom of the difference curve should represent the shape of the broad component, so that the area in region IV will represent an additional change in the narrow component. Calculations which depend on the position of the dotted line will take into account the possible error in positioning it. The points at which the difference curve begins to turn upward (A and B in Figure 10(b)) should represent the maximum width of the narrow component, and the solid line between points A and B should represent the actual shape of the narrow component, from which the half-width (width of the curve at half maximum) may be computed.

When using the difference curve method to compare curves, it must be assumed that the shapes of the narrow and broad components do not change and that the observed changes arise from changes in the intensity of the two components. This is a reasonable assumption when one considers the origin of the narrow and broad components. For example, the narrow

component is believed to arise from the annihilation of singlet positronium and any changes in the narrow component would be due to a change in the amount of positronium formed in the material. If the positronium thermalization efficiency changed, then the shape of the narrow component would change; but this is unlikely.

Figure 10(a) shows the curves for Teflon taken at 165°C and at 29°C. It is seen that the high temperature curve is narrower than the room temperature curve. This means that due to the increase in temperature some counts were transferred from the wings of the curve to the peak. The difference curve shown in Figure 10(b) has a central area which is (5.2 ± 2)% of the total area of the Teflon curve. This means that if the assumption that the narrow component is entirely due to annihilation of singlet positronium is correct, then 5.2% more positrons formed positronium at 165°C than at 29°C. If the assumption is made that no $^3S_1$-$^1S_0$ conversion contributes to the narrow component, then the change in I_2 is

$$I_2 = 3 \times (5.2 \pm 2)\% = (15.6 \pm 6)\%.$$

From the difference curve the half-width of the narrow component is 2.7 ± .2 milliradians. The error limits were determined from statistical errors in the count rate and from possible error in positioning the dotted line of the difference curve. However, the position of the dotted line does not affect the half-width measurement.

The half-width of the broad component may be found from the portion of the difference curve which lies below the zero line. However, the value one obtains depends heavily on the shape of the dotted portion of the curve. A more reliable method of determining the half-width of the broad component will be discussed in Chapter IV. It should be mentioned

that in the method for finding the percent of change of the narrow component, the shape of the dotted portion of the curve is not critical since most of the region under consideration is defined by the experimental points.

Using the relations $\theta = \frac{P}{m_0 c}$ and $P = \sqrt{4 m_0 E}$ to give $E = \frac{m_0 c^2 \theta^2}{4}$ and substituting

$$\theta = \frac{\text{measured half-width of narrow component}}{2}$$

gives an average kinetic energy of the positronium at the time of annihilation of .23 ev, or about ten times thermal energy. Also, from the half-width of the broad component (obtained in Chapter IV), the average kinetic energy of the bound electrons in Teflon is

$$E = \frac{m_0 c^2 \theta^2}{4} = 4.35 \text{ ev.}$$

Figure 11(a) shows the curves for polystyrene taken at 70°C, 29°C, and -150°C. In order that the count rate might be increased, the -150°C curve was taken with a wider slit width (1.25 milliradians). This gave a broader curve than a narrow slit would have given, but this was corrected by an increase in the horizontal correction factor (see Appendix B, part B). This correction factor raises the points near the peak and lowers the points in the wings, so that the measured curve is made narrower. A separate background curve was also obtained with the wider slits and corrected for resolution effects using the new correction factor. These polystyrene curves are consistent with the Teflon curves in that a decrease in temperature gives a broader curve. It should be noted that the curves cross at approximately the same point, which seems to justify the assumption that the intensity of the individual components is changing, but not the shapes. Table I lists the values

obtained for the half-width of the narrow component and for the change in I_2. The narrow component half-width is about 5.5 milliradians which corresponds to a positronium kinetic energy of .93 ev.

Finally, Figure 12(a) shows the curves for Lucite taken at 29°C and -150°C. The low temperature Lucite curve was also taken with a slit width of 1.25 milliradians. From the difference curve the half-width of the narrow component is 7.0 ± 1.5 milliradians which gives a positronium kinetic energy of 1.56 ev.

C. Crystalline Quartz and Fused Quartz

Figure 13(a) shows the curves for crystalline quartz and fused quartz. These data may also be interpreted as a temperature effect in quartz since fused quartz is obtained by heating crystalline quartz to about 1500°C. The difference curve shows that (18.8 ± 2)% of the counts were transferred into the narrow component, so that

$$I_2 = 3 \times (18.8 \pm 2)\% = (56.4 \pm 6)\%.$$

This result is in good agreement with the value (53 ± 8)% obtained by Green and Bell (28) from lifetime measurements. The half-width of the narrow component is 3.2 ± .3 milliradians which leads to E_{pos} = .31 ev.

TABLE I

RESULTS OF THE DIFFERENCE CURVE CALCULATIONS

Material	Half-width: Narrow Component (mrad.)	Half-width: Broad Component (mrad.)	Average Kinetic Energy of Positronium at Time of Annihilation (ev)	Average Kinetic Energy of Valence Electrons (ev)	ΔI_2 (%)
Teflon (1)	2.7 ± .2	12.3 ± .5	.23 ± .03	4.34 ± .8	15 ± 5
Polystyrene (2)	6.0 ± 1.0		1.15 ± .3		10 ± 5
Polystyrene (3)	5.0 ± 1.0	8.7 ± 1.0	.80 ± .3	2.42 ± .9	15 ± 7
Polystyrene (4)	5.4 ± 1.0	8.8 ± 1.0	.93 ± .3	2.47 ± .9	24 ± 7
Lucite (5)	7.0 ± 1.5	9.2 ± 1.5	1.56 ± .5	2.70 ± 1.0	30 ± 10
Fused Quartz	3.1 ± .2	11.1 ± .4	.31 ± .03	3.94 ± .6	56 ± 6*
Crystalline Quartz	---	10.9 ± .2	---	3.80 ± .4	---

(1) Values calculated from the 29°C - 165°C difference curve
(2) " " " " 29°C - 70°C difference curve
(3) " " " " -150°C - 29°C difference curve
(4) " " " " -150°C - 70°C difference curve
(5) " " " " -150°C - 29°C difference curve

*Since crystalline quartz has no narrow component, this number gives the actual value of I_2 for fused quartz.

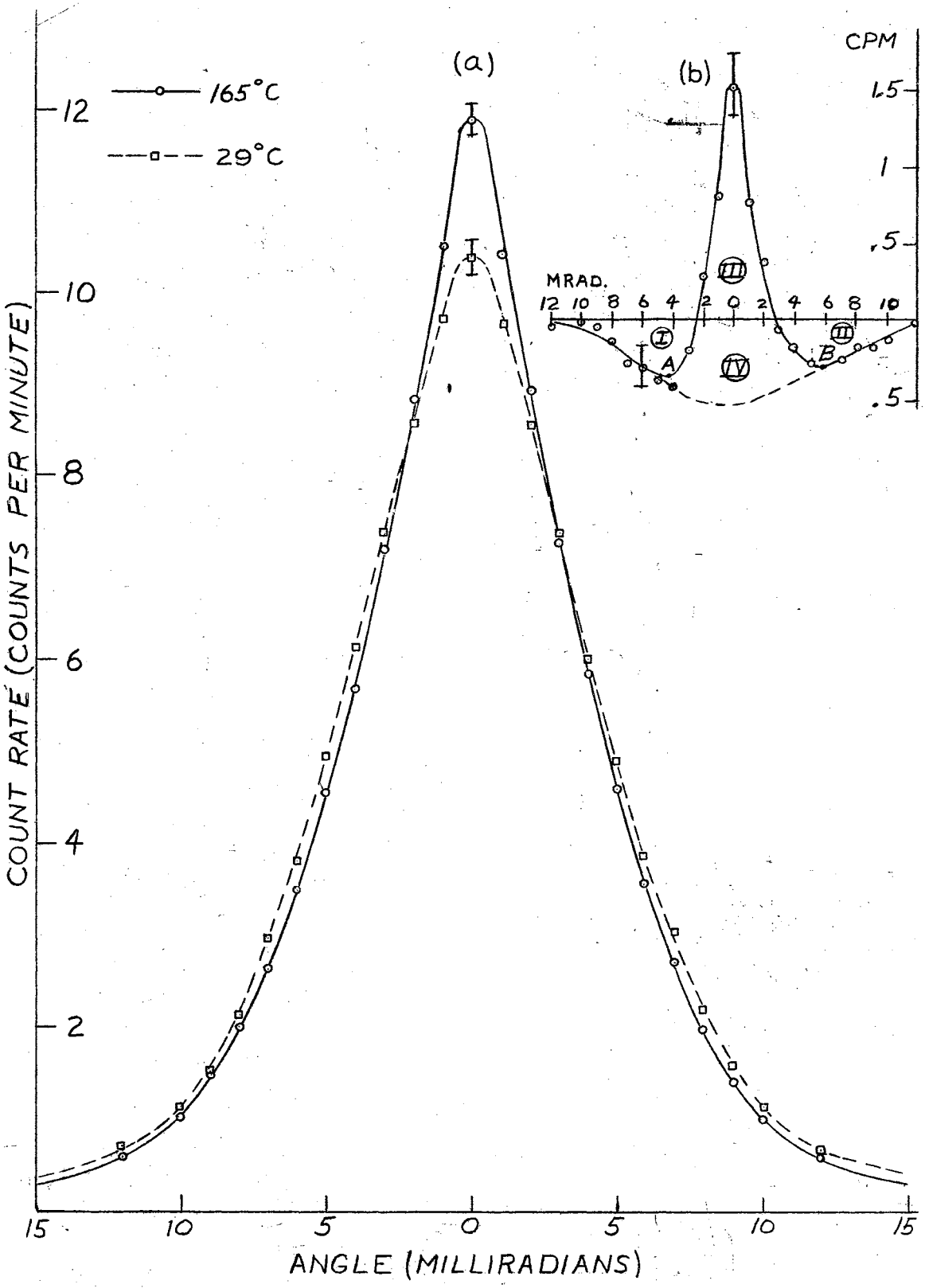

Figure 10. Angular Distribution of Annihilations in Teflon at 29°C and 165°C

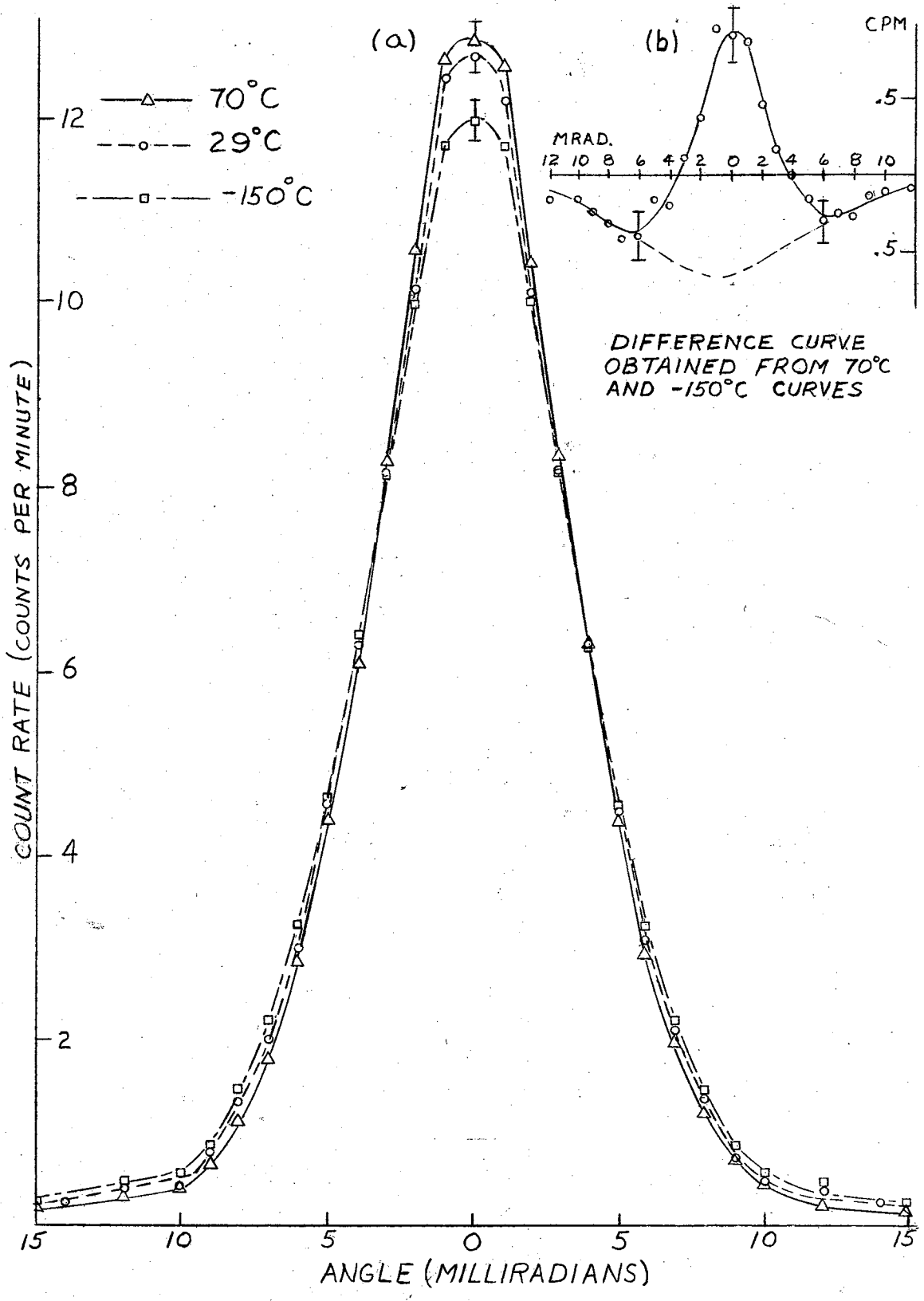

Figure 11. Angular Distribution of Annihilations in Polystyrene at -150°C, 29°C, and 70°C

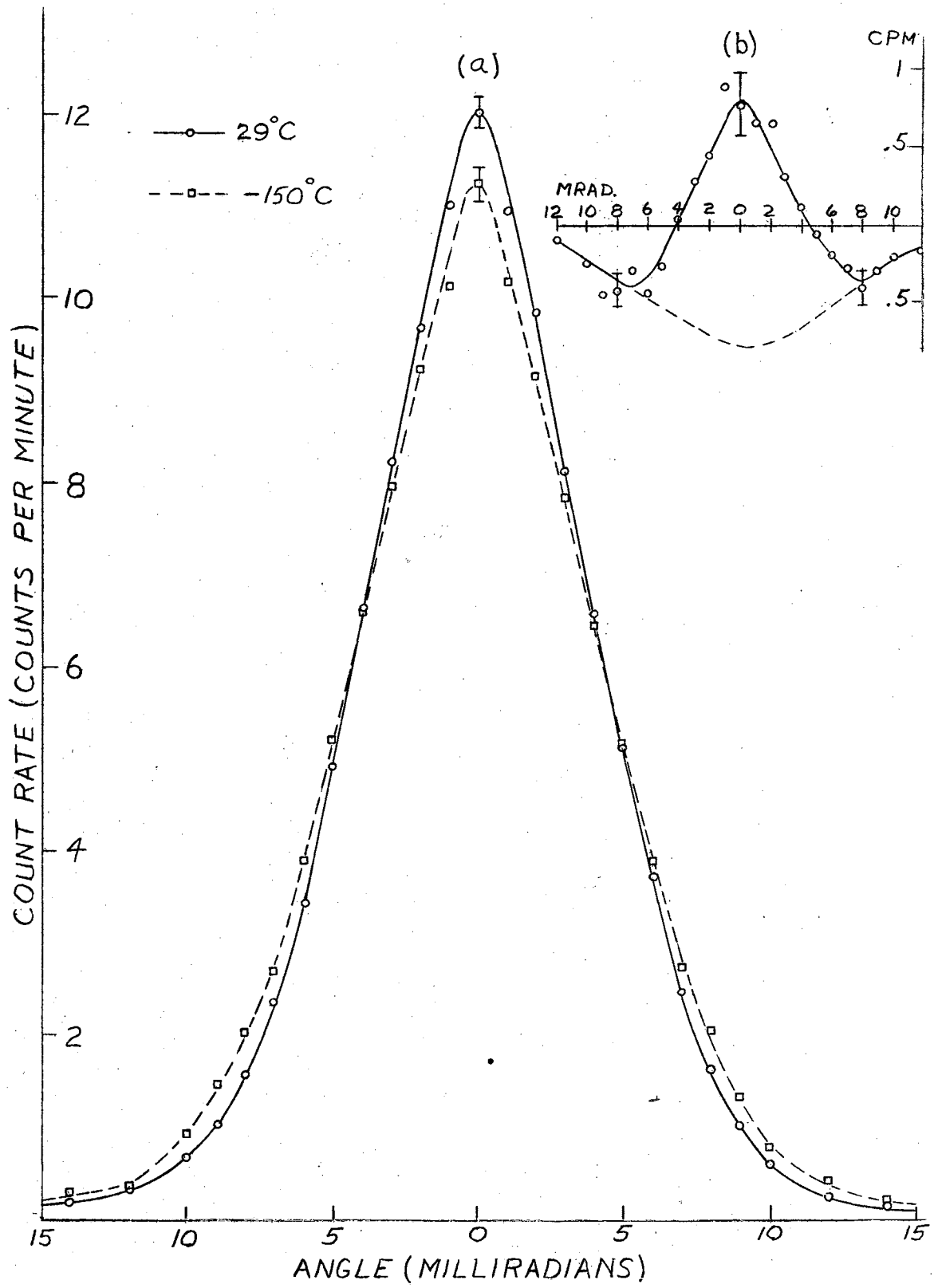

Figure 12. Angular Distribution of Annihilations in Lucite at -150°C and 29°C

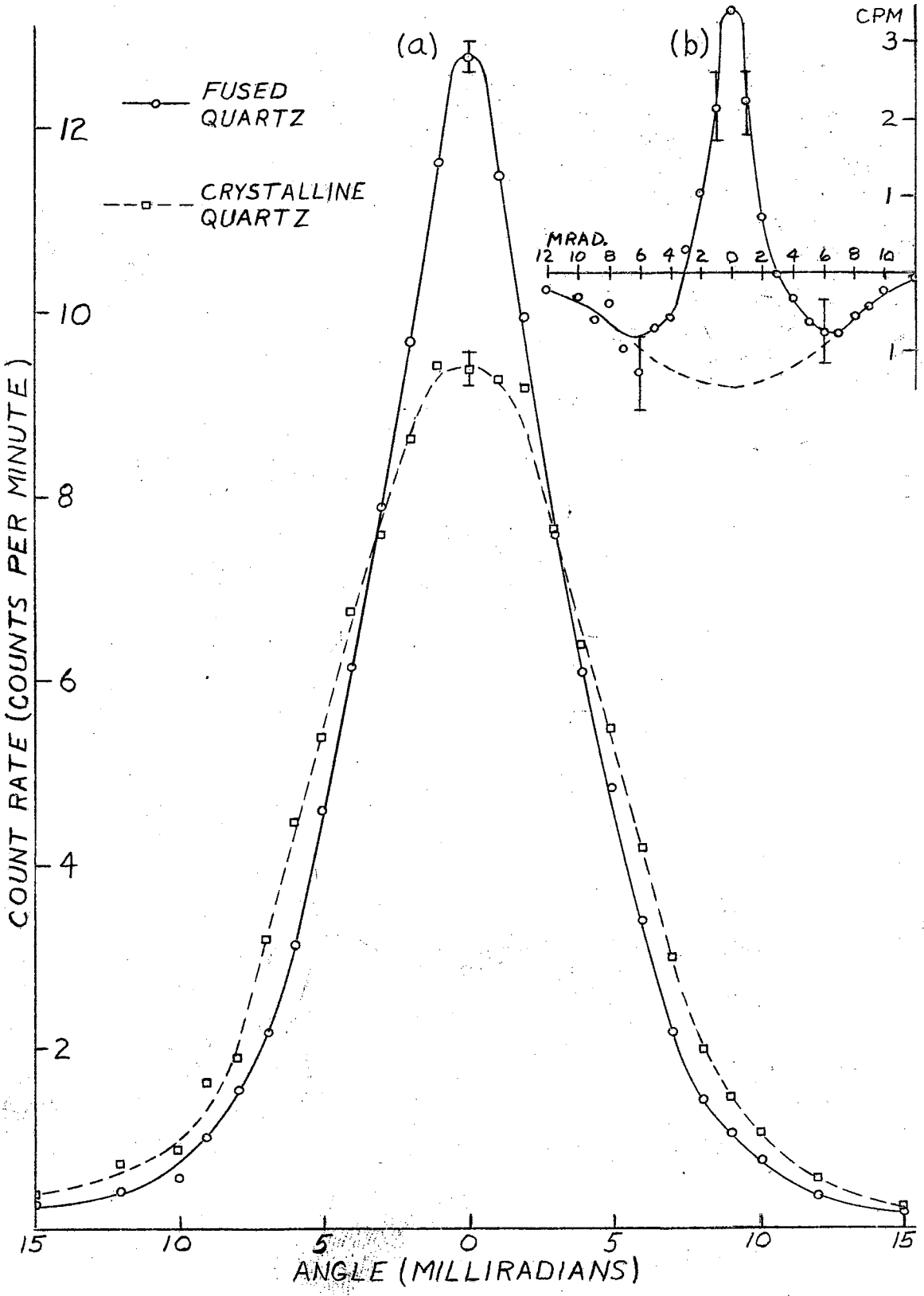

Figure 13. Angular Distribution of Annihilations in Fused Quartz and Crystalline Quartz

CHAPTER IV

DISCUSSION AND CONCLUSIONS

The experimental results show that at least in part, the temperature effect is actually a density effect. This explanation was first suggested by deZafra and Joyner (6) who also measured the effects of phase changes on materials exhibiting the τ_2 component of lifetime. The angular distribution narrows when the temperature is increased because the increased space between the molecules allows more positronium to be formed. De Benedetti, et.al. (22) have shown that the ground state energy of the positronium atom will become positive if the wave function is confined in a sphere of diameter less than 3.6 Å. As the spacing increases from this lower limit the positronium binding energy increases toward the free positronium binding energy of 6.8 ev. It is seen from Figure 1 that the width of the Ore gap is very dependent on the positronium binding energy; and if this binding energy increases, the width of the Ore gap increases. Opposing the increase in spacing caused by higher temperature is the increased molecular agitation. This would tend to break up a positronium atom and would also increase the probability of pickoff annihilation.

If the observed changes in I_2 are purely a density effect, then these changes should be related to the coefficients of thermal expansion of the materials. DeZafra and Joyner (6) have obtained peak rate vs.

temperature curves for Teflon, fused quartz and napthalene which show that within phase changes the change in I_2 is nearly linear. Assuming that this is also the case for polystyrene and Lucite, the percent of change in I_2 per degree may be calculated. The results are listed in Table II.

TABLE II

VARIATION OF τ_2 INTENSITY WITH TEMPERATURE

Material	$I_2/^oC$	Thermal Coefficient of Expansion, $10^{-5}/^oC$
Teflon	.11 ± .04	5.5
Polystyrene	.11 ± .04	6.0
Lucite	.16 ± .06	7.0

For these materials in the solid phase it is seen that within the limits of error the variation of positronium formation with temperature is the same. The fact that all three materials have nearly the same coefficient of thermal expansion is evidence for density hypothesis.

From the calculations involving the narrow component half-width it is seen that Teflon has the greatest thermalization efficiency for positronium. This could mean that the positronium suffers more inelastic collisions in Teflon than in the other materials. It could also mean that the lifetime of singlet positronium is longer in Teflon than in the other materials. In any case the data show that the positronium is by no means thermalized (.025 ev) at the time of annihilation. Of the materials studied, Lucite seems to have the poorest positronium thermalization efficiency. This must be due to more tightly bound electrons and therefore more elastic collisions.

The calculations for the energy of the positronium atom at the time of annihilation are to be taken only as an approximation. These

calculations were made assuming the total momentum of the positronium atom to be in the Z direction (see Figure 2), whereas the angular correlation method measures only the Z-component of the momentum. However, most of the annihilations detected probably have a relatively small x-component, so that these results might be more accurate if they were increased by a factor of $\sqrt{2}$. This is also true of the results obtained for the average kinetic energy of the valence electrons. These values for the kinetic energy of the valence electrons are even more uncertain because of the assumption that the positron is completely thermalized and the assumption that only valence electrons are annihilating the positrons.

To find the shape and half-width of the broad component, which in turn will give an estimate of the mean kinetic energy of the outer electrons, the following method was used. As was mentioned in Chapter III, the point at which the difference curve begins to turn upward should represent the maximum width or the base width of the narrow component. The shape of the narrow component would then be defined by the points on the difference curve which lie between points A and B in Figure 10(b).

If it is assumed that the narrow component is composed entirely of annihilations from singlet positronium and that there is negligible $^3S_1 \rightarrow {}^1S_0$ conversion, then it is easily shown that the percent of annihilations in the narrow component is

$$N = \frac{I_2 f + 1}{3(f+1)} = \frac{I_2 + \frac{1}{f}}{3 + \frac{3}{f}},$$

where f is the ratio of 2γ annihilations to 3γ annihilations. For materials in which only free state annihilations occur, f = 372. For the materials used here, Pond (29) has measured $f \approx 130$. Therefore, to a good approximation, $N = \frac{I_2}{3}$.

Since its shape and base width are known, the narrow component may easily be drawn to include $\frac{I_2}{3}$ percent of the area of the measured distribution. The shape and half-width of the broad component may then be determined by subtraction. The value for I_2 must be obtained from lifetime measurements, except in the case of quartz, where it may be measured directly from the fused quartz-crystalline quartz difference curve. Figure 14 shows the fused quartz distribution with its narrow and broad components obtained in the manner described above. The half-width of the fused quartz broad component is 11.1 ± .4 milliradians which agrees very well with the half-width of the crystalline quartz curve which is 10.9 ± .2 milliradians. These results tend to confirm the assumption that the shapes of the individual components do not change, and that only their intensity changes with temperature. Another check on this method is to normalize the fused quartz broad component to the same area as the crystalline quartz curve. When this is done, the two curves are identical.

Figures 14-17 show the broad and narrow components for each material. If the materials are compared, it is seen that Teflon has the highest thermalization efficiency and also the most energetic valence electrons. Polystyrene and Lucite, on the other hand, have comparitively poor thermalization efficiency and the least energetic valence electrons. This indicates that the positronium atom loses more energy in a collision with a fast electron than with a slower one. Since the valence electrons in Teflon are moving more rapidly, they would not have as much time to interact with the positronium. This could explain why Teflon has a larger τ_2 lifetime component than polystyrene or Lucite. However, the question then remains as to why Teflon and polystyrene have the same τ_2

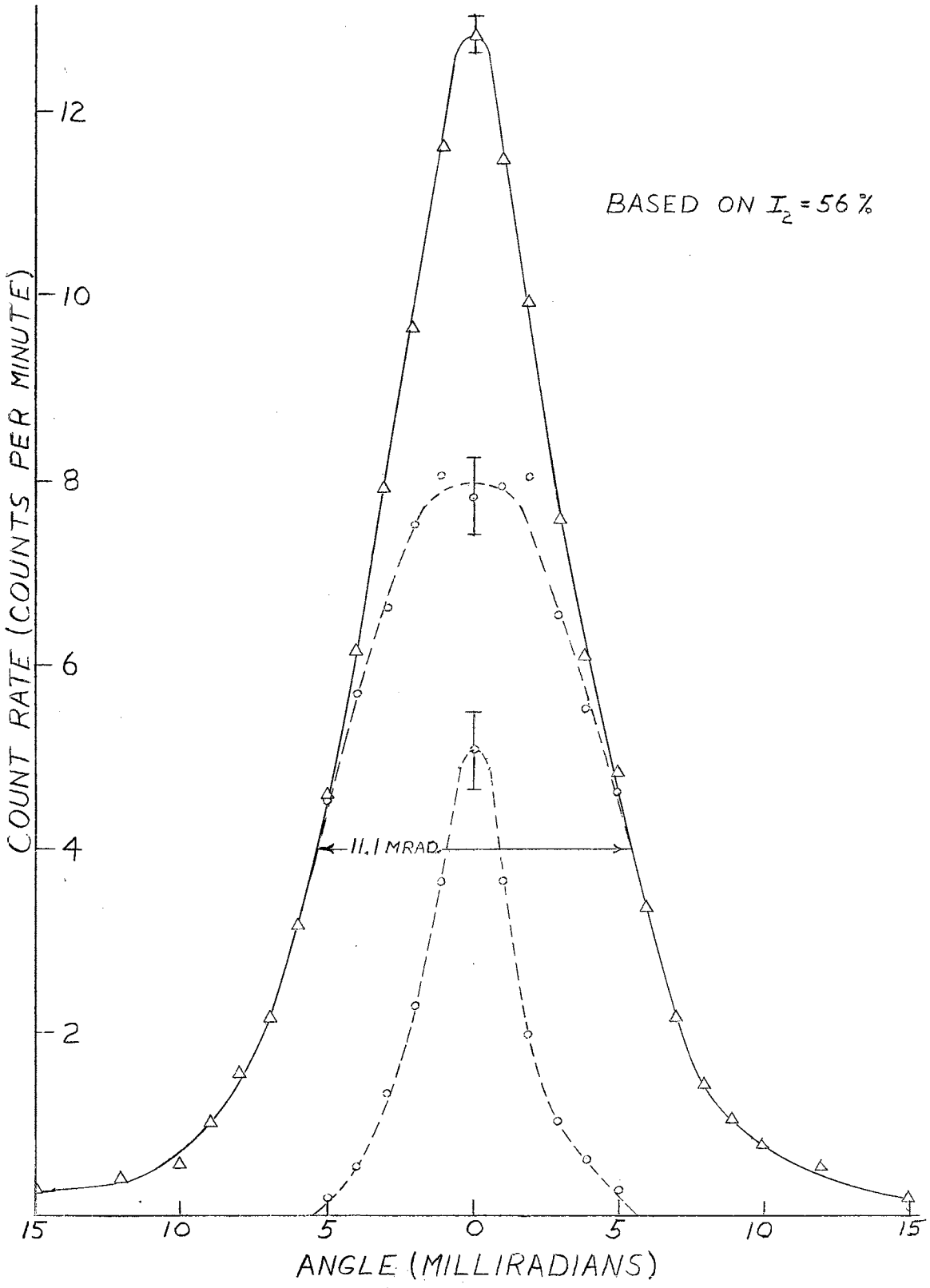

Figure 14. Angular Distribution of Annihilations in Fused Quartz at 29°C Showing the Broad and Narrow Components.

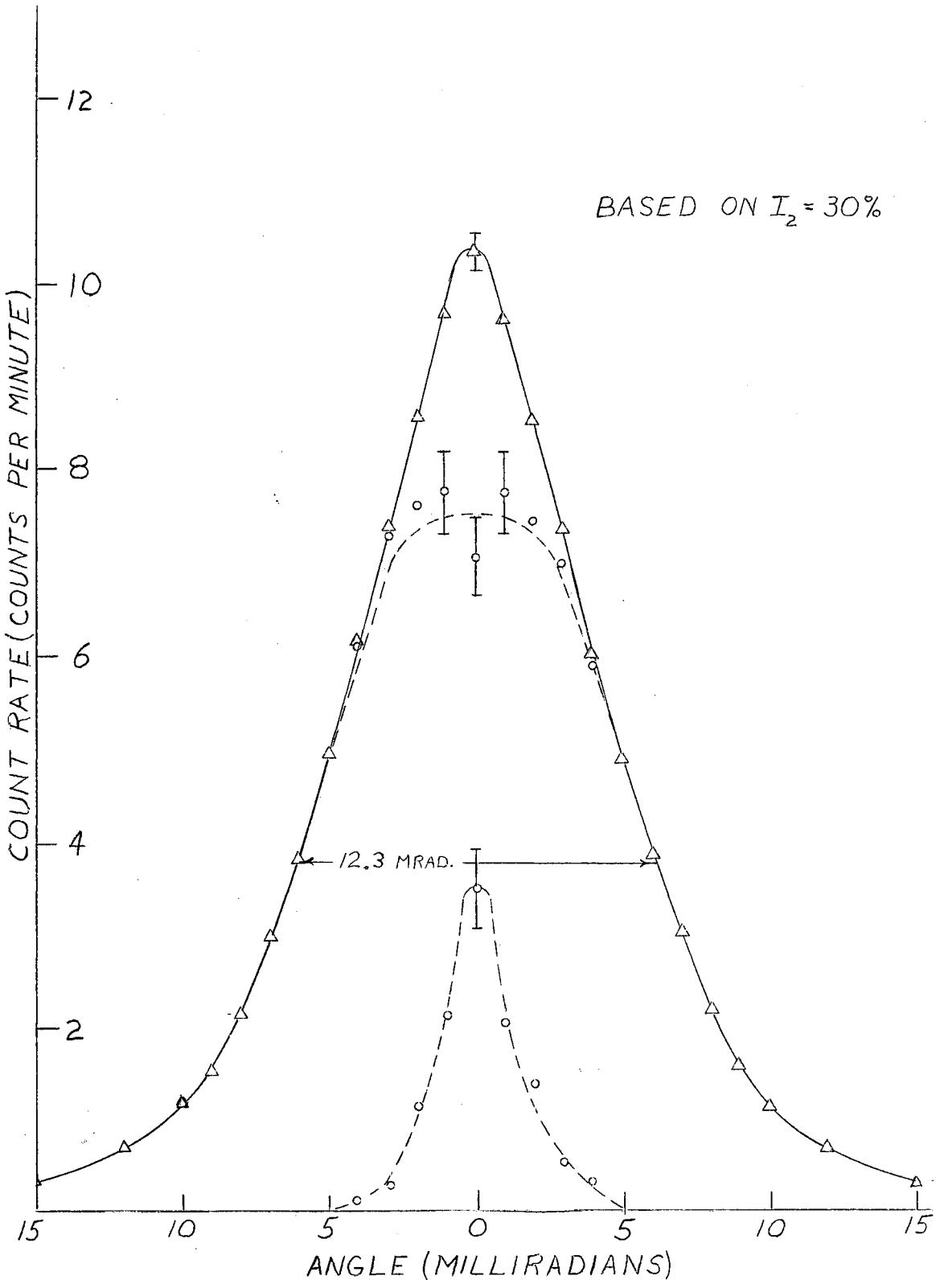

Figure 15. Angular Distribution of Annihilations in Teflon at 29°C Showing the Broad and Narrow Components.

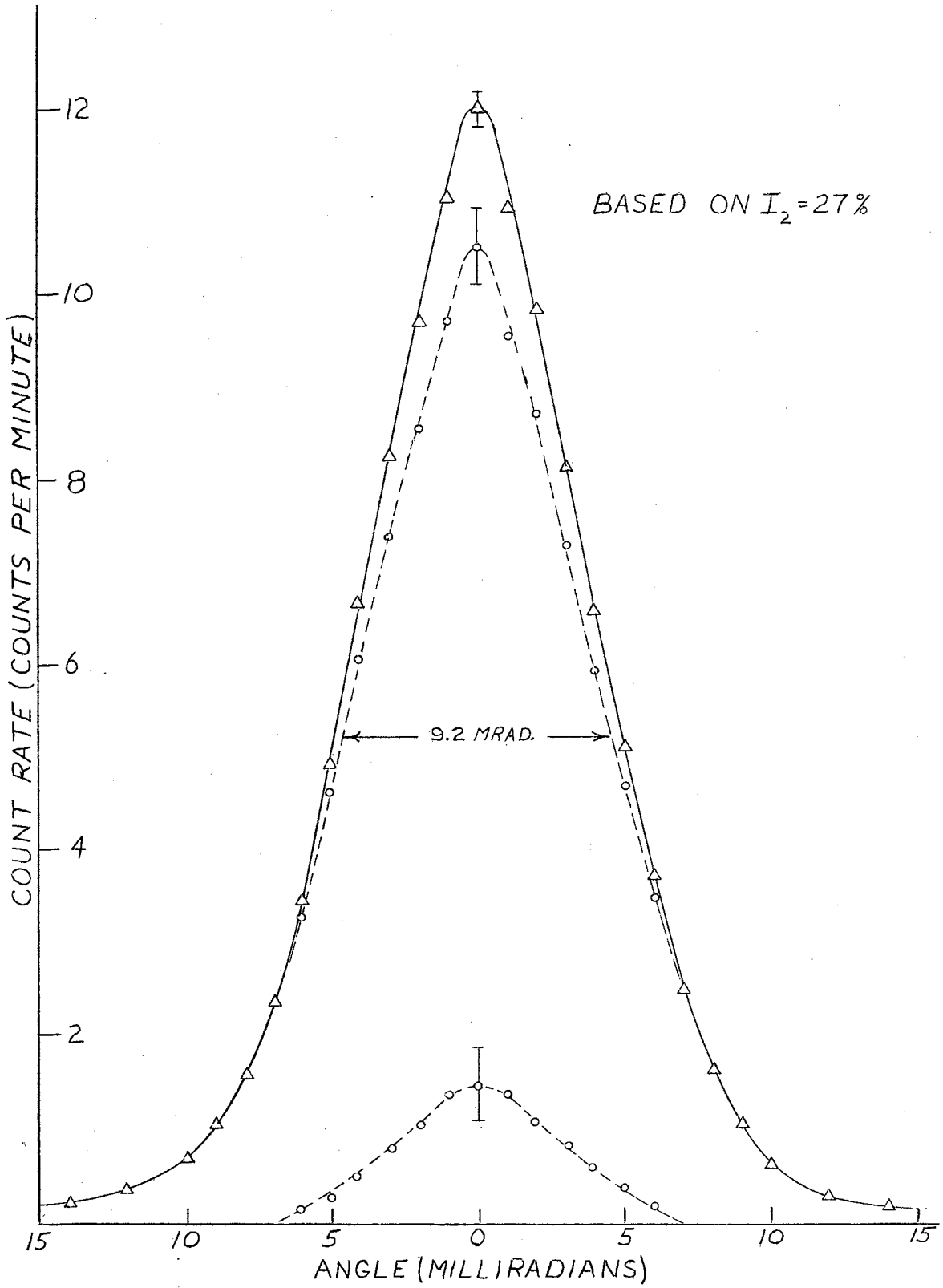

Figure 16. Angular Distribution of Annihilations in Lucite at 29°C Showing the Broad and Narrow Components.

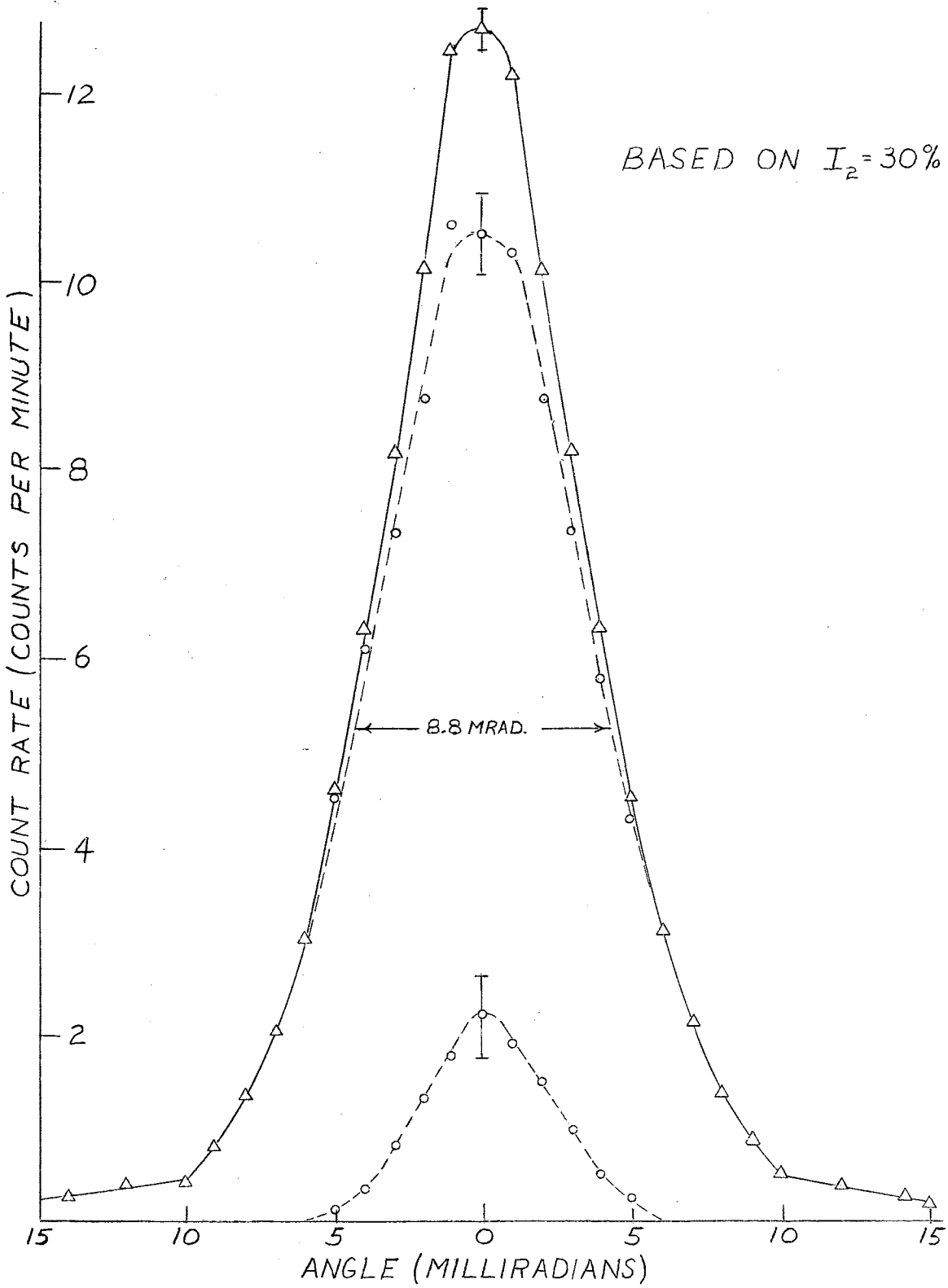

Figure 17. Angular Distribution of Annihilations in Polystyrene at 29°C Showing the Broad and Narrow Components.

lifetime at -196°C, even though the shape of their individual components does not change. A more likely explanation is that at room temperature Teflon has a greater free volume than polystyrene, and therefore more room for the positronium atom to "hide". The Teflon free volume would then have to decrease faster with temperature than the polystyrene free volume.

In order to answer these questions, this work should be extended to other materials and also to different temperatures of the materials used here. In particular it would be interesting to measure the change in I_2 in a material which had a different coefficient of thermal expansion than the materials used here. However, if the assumption that the change in I_2 is approximately linear throughout the solid phase is incorrect, this test would not be very meaningful. It would also be interesting to try to find a material which has both a wide narrow component and a wide broad component or one which has a narrow narrow component and a narrow broad component. The four materials studied here have either a narrow narrow component and a wide broad component or vice versa.

Since the differences to be measured are small, a better source geometry and also a stronger source should be used. Also, for low temperature work the method of cooling by conduction has not been satisfactory because too much heat enters the system and because the cooling liquid does not last long enough outside the dewar. In the future the sample and source should be immersed in the cooling liquid. This makes alignment more difficult but not impossible. The important thing is for the alignment to be rigid throughout a particular run. Another suggestion for future work would be to build an automatic

position changer with a recorder. This device could be programmed to change the position of the movable slit at regular intervals so that instrumental drift would not have as great an effect on the data.

BIBLIOGRAPHY

1. DuMond, J., D. Lind, and B. Watson: Phys. Rev., 75: 1226 (1949).
2. Berko, S. and F. Hereford: Revs. Mod. Phys., 28: 299 (1956).
3. Wallace, P.: Solid State Phys., 10: 1 (1960).
4. Heitler W.: The Quantum Theory of Radiation, (Oxford University Press, New York and London, 1936) p. 271.
5. Ferrell, R.: Revs. Mod. Phys., 28: 305 (1956).
6. DeZafra, R. and W. Joyner: Phys. Rev., 112: 19 (1958).
7. Garwin, R.: Phys. Rev., 91: 1571 (1953).
8. Bell, R. and R. Graham: Phys. Rev., 90: 644 (1953).
9. Deutsch, M.: Phys. Rev., 83: 866 (1951).
10. DeBenedetti, S. and H. Corben: Ann. Rev. Nuclear Sci., 4: 191 (1954).
11. Dirac, P.: Proc. Camb. Phil. Soc., 26: 361 (1930).
12. Wheeler, J.: Ann. New York Acad. Sci., 48: 219 (1946).
13. Ore A. and J. Powell: Phys. Rev., 75: 1696 (1949).
14. Basson, J.: Phys. Rev., 96: 691 (1954).
15. Deutsch, M.: Phys. Rev., 82: 455 (1951).
16. Dresden, M.: Phys. Rev., 93: 1413 (1954).
17. Good, W., D. Peaslee, and M. Deutsch: Phys. Rev., 69: 313 (1949).
18. Dicke, R. and J. Wittke: Introduction to Quantum Mechanics, (Addison-Wesley Publishing Co., London, 1960) p. 281.
19. Wallace, P.: Phys. Rev., 100: 738 (1955).
20. Jauch, J. and F. Rohrlich: The Theory of Photons and Electrons, (Addison-Wesley Publishing Co., Cambridge, 1955) p. 274.

21. Lang, G., S. DeBenedetti, and R. Smoluchowski: Phys. Rev., 108: 914 (1957).

22. DeBenedetti, S., C. Cowan, W. Konneker, and H. Primakoff: Phys. Rev., 77: 205 (1950).

23. Green, R. and A. Stewart: Phys. Rev., 98: 486 (1955).

24. Page, L., M. Heinberg, J. Wallace, and T. Trout: Phys. Rev., 98: 206 (1955).

25. Page, L. and M. Heinberg: Phys. Rev., 102: 1545 (1956).

26. Brandt, W., S. Berko, and W. Walker: Phys. Rev., 120: 1289 (1960).

27. Seigbahn, K.: Beta- and Gamma Ray Spectroscopy, (Interscience Publishers, Inc., New York, 1955) p. 202.

28. Green, R. and B. Bell: Can. J. Phys., 35: 398 (1957).

29. Pond, T.: Phys. Rev., 93: 478 (1954).

30. Condon, E. and H. Odishaw: Handbook of Physics, (McGraw-Hill Book Co., Inc., New York, 1959) Part 9. p. 117.

31. Pirenne, M.: The Diffraction of X-Rays and Electrons by Free Molecules, (Cambridge University Press, New York and London, 1946) p. 50.

32. Lang, G.: Ph.D. Thesis, Carnegie Institute of Technology, 1956 (unpublished).

33. Eckart, C.: Phys. Rev., 51: 735 (1937).

APPENDIX A

SCATTERING CORRECTIONS

Any scattering which the gamma rays undergo from the time of their creation until they reach the scintillation counters can distort the measured distribution. This scattering can take place in the sample or in the 200 cm. of air on each side of the sample. To make matters simpler it will be assumed that one photon has already reached one scintillation counter and the other must travel the full thickness of the sample (.6 cm.) and 400 cm. of air. Also, since the samples used were amorphous substances for which it is difficult to find tabulated values of scattering coefficients, these calculations will be carried out for lead, which is one of the most critical cases.

One scattering process which has a high probability for .51 Mev gammas is Compton scattering in the sample. This process is the interaction of a photon with an electron which is assumed to be free and at rest. This assumption neglects the small binding energy of the electrons to atoms and is valid provided the momentum transferred to the electron greatly exceeds the momentum of the electron in the bound state. The differential cross section per electron for Compton scattering is given by the Klein-Nishina formula (30) which is

$$\frac{d\sigma}{d\Omega} = \frac{r_o^2}{2} \cdot \frac{1+\cos^2\phi}{\left[1+\frac{h\nu_o}{m_oc^2}(1-\cos\phi)\right]^2} \left\{ 1 + \frac{\left(\frac{h\nu_o}{m_oc^2}\right)^2 (1-\cos\phi)^2}{(1+\cos^2\phi)\left[1+\frac{h\nu_o}{m_oc^2}(1-\cos\phi)\right]} \right\}.$$

where

r_o = classical electron radius = 2.82×10^{-13} cm.

ϕ = angle through which gamma ray is scattered

$h\nu_o$ = energy of photon = .51 Mev

$m_o c^2$ = rest energy of electron = .51 Mev

For photon energies of .51 Mev, $\frac{d\sigma}{d\Omega}$ is nearly symetrical about $\phi = \frac{\pi}{2}$. Substituting $\phi = 0$ and $\phi = 30$ milliradians into $\frac{d\sigma}{d\Omega}$ gives results which differ by less than .25%.

Since the measured distribution lies in a region between zero and twenty milliradians, the effect of Compton scattering would be very nearly the same at all points in the distribution. The percent of photons which are Compton scattered in .6 cm. of lead is

$$\left(1 - e^{-\mu_c x}\right) = \left[1 - e^{-(.75)(.6)}\right] = 36\%.$$

The fraction of photons which are Compton scattered in less than 20 milliradians is

$$\Delta = (.36)\frac{\frac{d\sigma}{d\Omega}\Big|_o \cdot \pi\left[(20 \times 10^{-3})\, r\right]^2}{\sigma_T \qquad r^2} = 1.2 \times 10^{-4},$$

where

σ_T = total Compton cross section = 2.9×10^{-25} cm.^{2}

$\frac{d\sigma}{d\Omega}\Big|_o$ = differential Compton cross section evaluated at $\phi = 0$, which gives 7.9×10^{-26} cm.^{2}/steradian

r = 200 cm.

This shows that less than .012% of the recorded events have been Compton scattered. Also, if the scattered photon loses more than 96 Kev in the collision, the discriminator will keep the photon from being counted.

Another type of scattering which can affect the measured distribution is coherent Rayleigh scattering (30). This occurs when the momentum transfer to the bound atomic electrons is small enough so that the atom remains in its ground state. The gamma radiation will be scattered with a definite phase relation between the incoming and scattered wave and the frequency of the incoming wave will be unchanged. The intensity of the radiation scattered by a particular atom is determined by summing the amplitudes of the radiation which is coherently scattered by each of the electrons bound in the atom. The intensity variation with angle is produced by the interference of these individual waves and depends on the relative positions of the electrons. For the forward direction, the differential cross section for this coherent Rayleigh scattering (31) is

$$\left.\frac{d\sigma}{d\Omega}\right|_0 = \frac{1}{2} r_0^2 (1 + \cos^2\phi) Z^2,$$

where

Z = atomic number of sample.

As in the previous case of Compton scattering, $\frac{d\sigma}{d\Omega}$ varies only slightly from $\phi = 0$ to $\phi = 30$ milliradians. The percent of gamma rays which will be Rayleigh scattered is (for Pb)

$$\left(1 - e^{-\mu_{Ry} x}\right) = \left[1 - e^{-(.077)(.6)}\right] = 4.5\%.$$

Therefore the fraction of photons which are Rayleigh scattered in 20 milliradians is

$$\Delta = (.045)\frac{\left.\frac{d\sigma}{d\Omega}\right|_0}{\sigma_{T(Ry)}} \cdot \frac{\pi\left[(20 \times 10^{-3}) r\right]^2}{r^2}$$

or

$$\Delta = .012.$$

This shows that less than 1.2% of all recorded events have been Rayleigh scattered.

G. Lang (32) estimates that scattering in the 400 cm. of air introduces a maximum error at any point of the measured distribution of .2% of the peak rate.

Thompson scattering and the various types of nuclear scattering have comparitively low cross sections for .51 Mev gamma rays, so that they need not be considered.

APPENDIX B

RESOLUTION FUNCTIONS

A. Vertical Resolution

Due to the fact that the NaI crystals have a finite width in the vertical direction (a very small width or an infinite width would be ideal), a "vertical resolution" curve must be plotted. The purpose of this curve is to determine the error introduced due to the fact that for a given position of the movable counter there will be less coincidences between photons of large angular deviation from 180 degrees than between photons with smaller angular deviation from 180 degrees (see Figure 18).

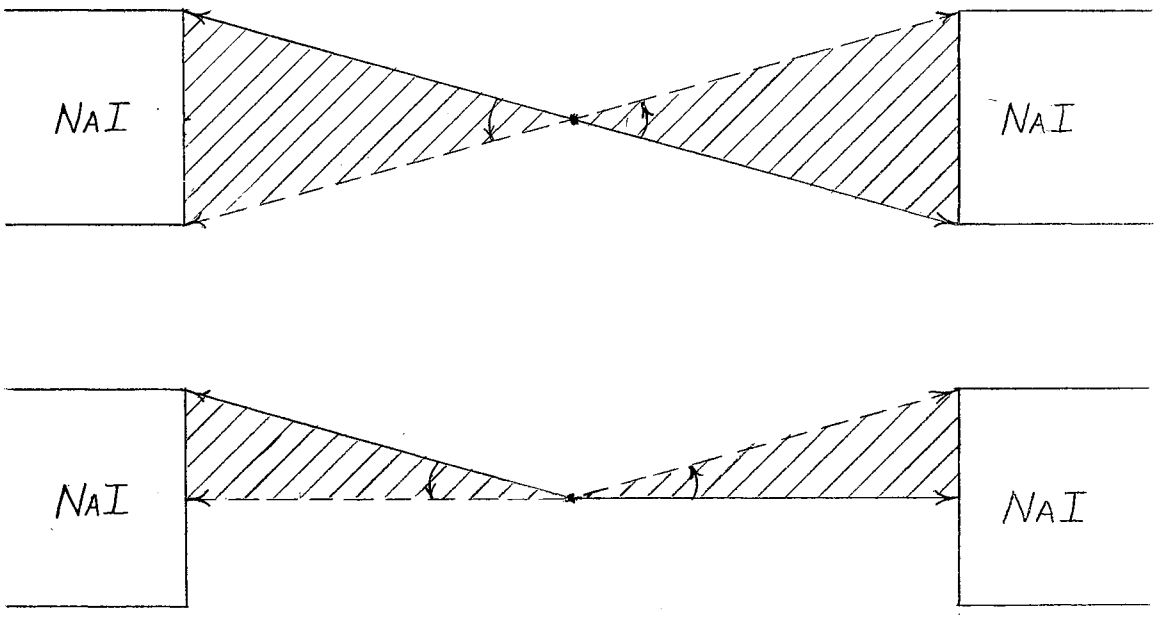

Figure 18. Vertical Resolution

The most critical position of the movable counter is the zero position. In this position a coincidence may be registered for angles ranging from zero to 44 milliradians; whereas at the 10 milliradian position, no coincidences of less than 10 milliradian deviation will be detected. Therefore, the vertical resolution function will be derived only for the zero position, since it is the most critical one. For the point source shown in Figure 18 the resolution function would simply be a triangle with a base half-width equal to the width of the detector divided by the distance of the detector from the source, so that for our geometry,

$$\text{base half width} = \tan \phi = \frac{5}{200} = 25 \text{ milliradians.}$$

The height of the triangle is arbitrary and should coincide with the peak of the measured distribution. Since the source used was not a point but had a vertical extension 3.8 cm., any point a distance H from the center of the source gives rise to a similar triangular function; so that the total vertical resolution function will be obtained by summing the infinitely many triangles which arise as H varies from the top to the bottom of the source (Figure 19). It must be assumed that the Na^{22} is evenly distributed on the mylar.

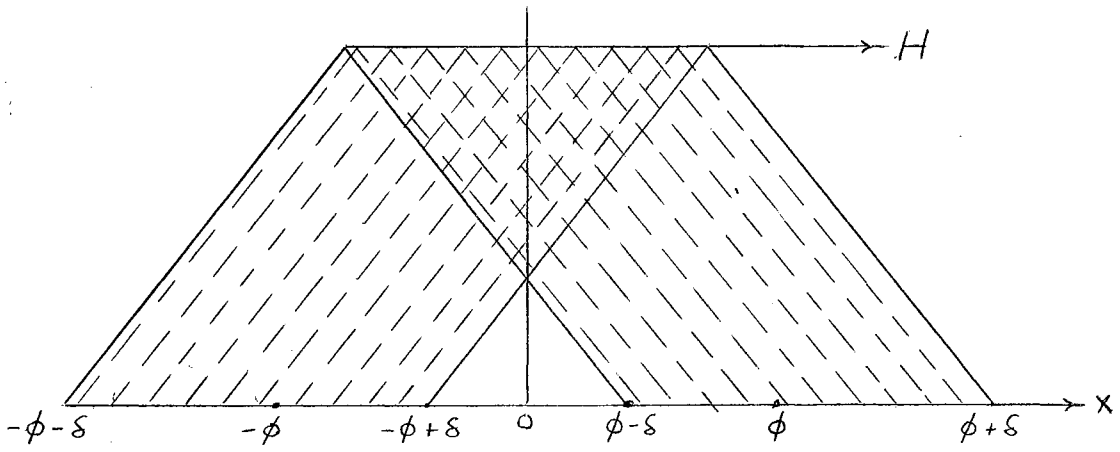

Figure 19. Distribution of Point Source Functions in the Vertical Direction

The maximum value of H is

$$H_{max} \equiv \delta = \frac{3.8 \text{ cm.}}{200 \text{ cm.}} = 19 \text{ milliradians},$$

so that H varies from -19 to 19 milliradians.

The expression for any particular triangle of height ϕ is given by

$$f(x,H) = [\phi - |H-x|], \quad H-\phi \leq x \leq H+\phi$$

and the total vertical resolution function is

$$F(x) = \int_{-\delta}^{\delta} f(x,H)dH = \int_{\delta}^{\delta} [\phi - |H-x|]\,dH.$$

This expression cannot be integrated directly because of the absolute value in f(x,H). Therefore, f(x,H) must be divided up into regions, so that the absolute value sign may be removed. This gives rise to two functions:

$$f_1(x,H) = [\phi - (H-x)], \quad \text{positive slope}$$
$$f_2(x,H) = [\phi - (x-H)], \quad \text{negative slope}.$$

Since the final function F(x) will be symetrical about zero, only the positive half of the curve will be integrated. Considering Figure 19, the integrals are

$$F_1(x) = \int_{-\delta}^{x} [\phi - (x-H)]dH + \int_{x}^{\delta} [\phi - (H-x)]\,dH, \quad 0 \leq x \leq \phi - \delta$$
$$F_2(x) = \int_{x-\phi}^{x} [\phi - (x-H)]dH + \int_{x}^{\delta} [\phi - (H-x)]\,dH, \quad \phi - \delta \leq x \leq \delta$$
$$F_3(x) = \int_{x-\phi}^{\delta} [\phi - (x-H)]dH, \quad \delta \leq x \leq \phi + \delta$$

The limits are chosen so that the term in parenthesis, (x-H) or (H-x), will always be positive and less than ϕ. Evaluating these integrals gives

$$F_1(x) = 2\phi\delta - \delta^2 - x^2, \quad 0 \leq x \leq \phi - \delta$$
$$F_2(x) = \frac{1}{2}(\phi^2 - \delta^2) + \delta\phi - (\phi - \delta)x - \frac{x^2}{2}, \quad \phi - \delta \leq x \leq \delta$$
$$F_3(x) = \frac{1}{2}(\phi + \delta)^2 - (\phi + \delta)x + \frac{x^2}{2}, \quad \delta \leq x \leq \phi + \delta$$

The total vertical resolution function is plotted in Figure 20. If the angular distribution of Teflon (one of the most critical cases) is plotted on the same axes, and the product $F(x)\gamma(x)$ is integrated from zero to 15 milliradians and compared with the integral of $G(x)\gamma(x)$ over the same limits, the two integrals differ by about four percent. This means that for the zero position, the number of coincidence counts that are missed due to the finite width of the detector is four percent of the peak rate. For positions away from zero, the percent missed is much less than at zero. Although the percent missed changes slightly for different samples, this small difference will be neglected in making corrections. All curves shown have had their peaks increased by four percent and all other points increased by proportionately smaller percentages.

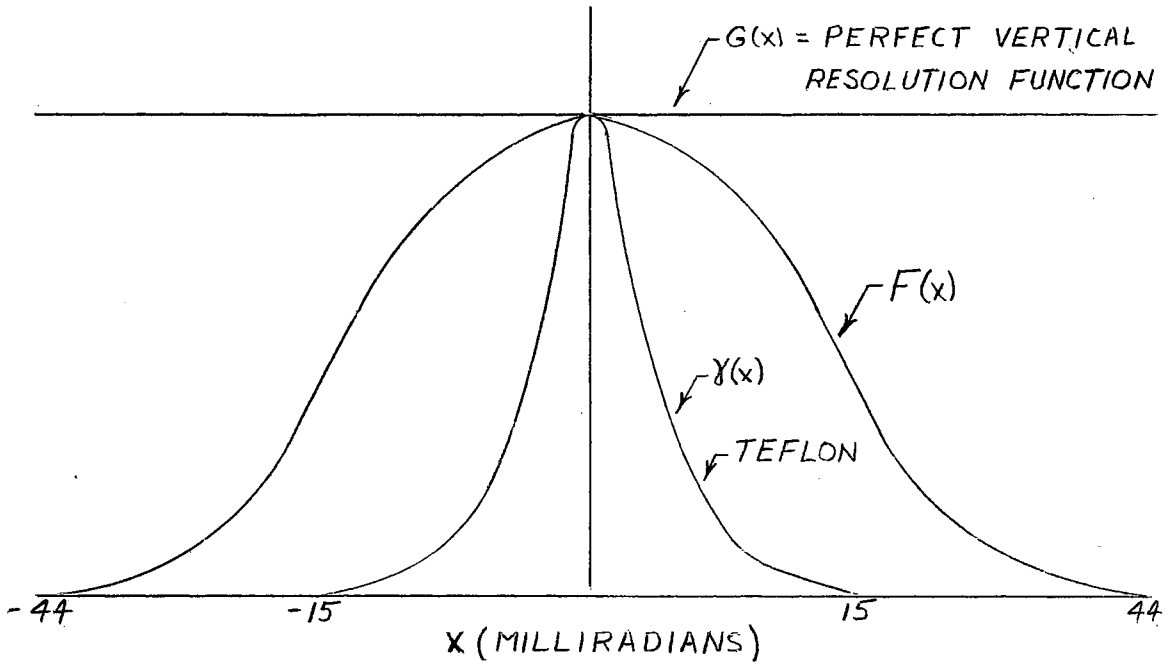

Figure 20. Vertical Resolution Function

B. Horizontal Direction

The method used for finding the horizontal resolution function is exactly the same as for the vertical direction. The approximate width of the source is 2.5 millimeters so that $\delta = \frac{2.5}{200} = 1.25$ milliradians. The slit width used was 1.3 millimeters so that $\phi = \frac{1.3}{200} = .65$ milliradians. A plot of the triangular functions obtained as H varies from $-\delta$ to δ is shown in Figure 21.

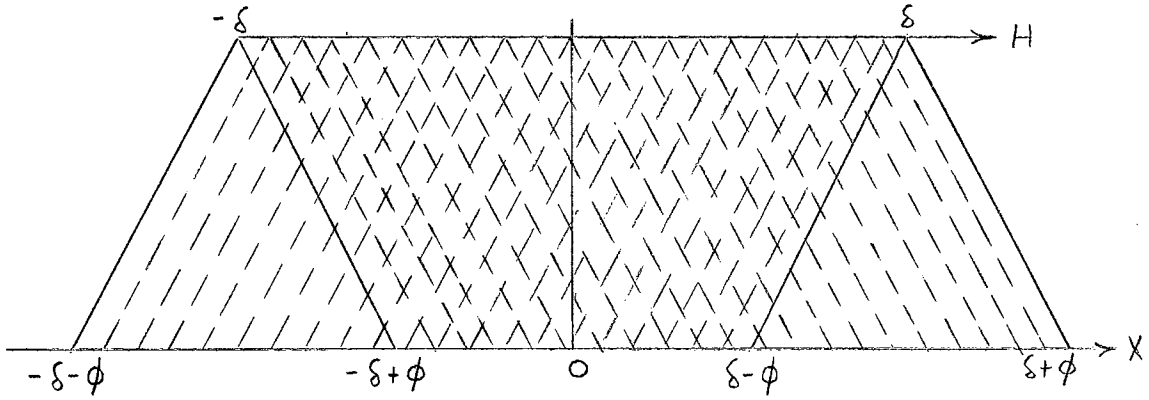

Figure 21. Distribution of Point Source Functions in the Horizontal Direction

The integrals for the positive region are

$$F_1(x) = \int_{x-\phi}^{x} [\phi - (x-H)]\, dH + \int_{x}^{x+\phi} [\phi - (H-x)]\, dH , \qquad 0 \le x \le \delta - \phi$$

$$F_2(x) = \int_{x-\phi}^{x} [\phi - (x-H)]\, dH + \int_{x}^{\delta} [\phi - (H-x)]\, dH , \qquad \delta - \phi \le x \le \delta$$

$$F_3(x) = \int_{x-\phi}^{\delta} [\phi - (x-H)]\, dH , \qquad \delta \le x \le \delta + \phi .$$

Integrating these expressions gives

$$F_1(x) = \phi^2 , \qquad 0 \le x \le \delta - \phi$$

$$F_2(x) = \tfrac{1}{2}(\phi^2 - \delta^2) + \delta\phi + (\delta - \phi)x - \frac{x^2}{2} , \qquad \delta - \phi \le x \le \delta$$

$$F_3(x) = \tfrac{1}{2}(\phi + \delta)^2 - (\phi + \delta)x + \frac{x^2}{2} , \qquad \delta \le x \le \delta + \phi .$$

The total horizontal resolution function is plotted in Figure 22.

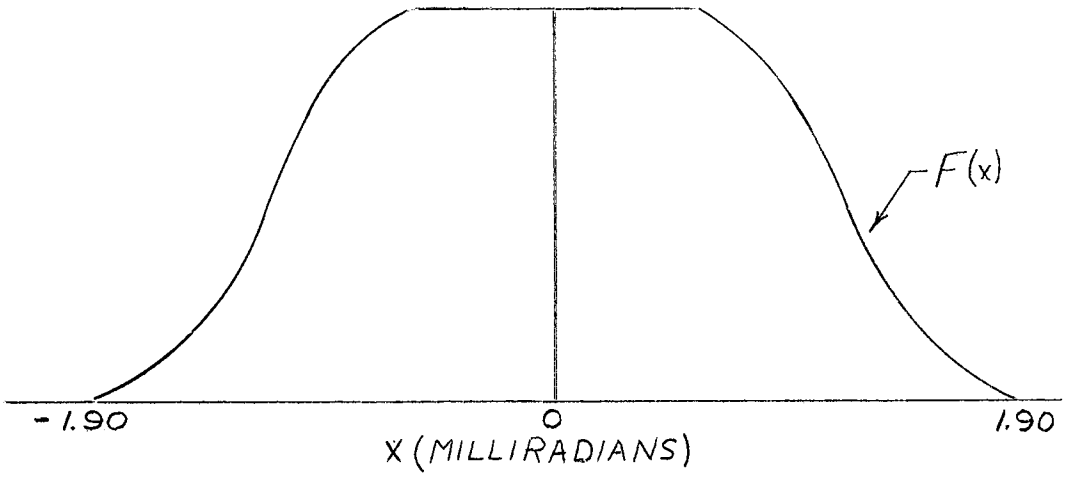

Figure 22. Horizontal Resolution Function

The correction which must be made for each particular point on the measured distribution curve is given by (33)

$$\rho_n = I_n - \mu\left[\frac{I_{n+1} + I_{n-1}}{2} - I_n\right],$$

where

μ = moment of inertia of horizontal resolution function $= \dfrac{\int_0^{\phi+\delta} X^2 F(x)\,dx}{\int_0^{\phi+\delta} F(x)\,dx}$

$F(x)$ = horizontal resolution function

$I_0, I_1, \ldots I_n$ = counting rates measured at 0, 1, ...n milliradians

ρ_n = corrected value of I_n.

In our case the moment of inertia is

$$\mu = 0.606.$$

In the nearly linear regions of the measured distribution this horizontal correction is negligible. In the large angle region where the distribution begins to level off the correction is on the order of five percent or about .1 counts per minute. Near the peak the correction is about 3%. All curves shown have been corrected in the non-linear regions.

VITA

Lewis Porter Keller

Candidate for the Degree of

Master of Science

Thesis: TEMPERATURE EFFECTS ON THE ANGULAR CORRELATION OF POSITRON ANNIHILATION RADIATION IN SOLIDS

Major Field: Physics

Biographical:

Personal Data: Born July 25, 1938, in Valparaiso, Indiana, the son of Madeline and Charles D. Keller.

Education: Attended grade school and high school in Valparaiso, Indiana, and graduated in 1956. Received Bachelor of Science degree with a major in Physics from Valparaiso University in May 1960. Completed requirements for a Master of Science degree from Oklahoma State University, with a major in Physics, in August, 1962.